이학석사학위논문

Sequence Stratigraphy and Chemostratigraphy of the Cambrian Sesong and Hwajeol formations (Taebaek area) and the Machari Formation (Yeongweol area), Gangweon Province, Korea: Implications for a Mixed Carbonate-siliciclastic Environment of Stable Cratonic Interior

캄브리아기 태백지역의 세송, 화절층과 영월지역의 마차리층의 순차층서학과 화학층서: 안정된 내륙해의 혼합된 탄산염 쇄설성 환경에 대한 고찰

2017년 2월

서울대학교 대학원

지구환경과학부

김 윤 종

ABSTRACT

The focus of this study is application of sequence stratigraphy and chemostratigraphy to the Sesong and Hwajeol formations (Taebaek area) and the Machari Formation (Yeongweol area), which are interpreted to have deposited in mixed carbonate-siliciclastic stable craton interior during the upper Cambrian Series 3 to Furongian. The Sesong and Hwajeol formations consist of nine lithofacies, and seven lithofacies are recognized in the Machari Fromation based on facies analysis. According to the facies stacking pattern and the recognition of bounding surface, the Sesong and Hwajeol formations are comprised of three stratigraphic sequences with two bounding surfaces, and the Machari Formation consists of two stratigraphic sequences with a sequence boundary. Trace elements suggestive of redox condition are analyzed in the Machari Formation. Stable carbon isotope values of whole rock sample, which imply relative sea-level fluctuation, are analyzed in the Sesong and the overlying Hwajeol formations. The Sesong and Hwajeol formations (Taebaek area) and Machari Formation (Yeongweol area) are well correlated based on sequence stratigraphy, chemostratigraphy, and biostratigraphy. Stratigraphic sequences and bounding surfaces are compared with those of Gushan and Chaomidian formations in Shandong region, China. Sequence stratigraphic correlation between the two regions suggests that a basin-scale correlation is possible with sequence-bounding surfaces developed in stable cratonic interior basins characterized by mixed carbonate-siliciclastic environment. Sequence stratigraphic interpretation of this region suggest that the interplay

between carbonate productivity and siliciclastic sediment input and complexity of this setting of mixed carbonate-siliciclastic environments in stable cratonic interior differs from traditional models

Key Words: Cambrian, Mixed carbonate-siliciclasitc environment, Stable cratonic interior, Sequence stratigraphy, Chemostratigraphy, Stable carbon isotope, Redox-induced trace elements, Siliciclastic input, Carbonate productivity

TABLE OF CONTENTS

LIST OF FIGURES

LIST OF TABLES

1. Introduction

A depositional model of a mixed carbonate-siliciclastic environment is poorly understood. Carbonate production and terrigenous input are mutually exclusive. Terrigenous material influences carbonate production by reducing light penetration and clogging up feeding mechanism of animals and plants (Catuneuanu et al. 2011). Increasing of terrigenous input results in decreasing of carbonate production. Recently, new perspective models on a mixed carbonate-siliciclastic setting, especially in the inner detrital belt of Laurentia, are suggested based on detailed sedimentological, lithostratigraphic, biostratigraphic, and sequence stratigraphic data (Runkel et al. 1998, 2007; Myrow et al. 2012; Labaj and Prett 2016). Myrow et al (2012) proposed upward-deepening cycle in the intra-cratonic inner detrital belt. They interpreted upward-increasing carbonate of the cycle as the upward-deepening cycle, which is generated by transgression during dcreasing of the input of siliciclastic mud due to landward shoreline migration and river alluviation. Carlucci et al (2014) indicated the high-resolution cycle of Bromide Formation of Oklahoma deposited in a mixed carbonate-siliciclastic ramp.

Based on Paleogeographic reconstruction, A close affinity and a similarity of stratigraphy between the Taebaeksan basin and the North China Platform is suggested during the early Paleozoic (Chough et al., 2000; Kim and Lee, 2000; Choi et al., 2001; Kwon et al., 2006). Both strata of the Taebaeksan basin and the North China Platform was deposited in mixed carbonate-siliciclastic environment of a stable equatorial to subequatorial craton; thus the

Taebaeksan basin and the North China Platform have experienced similar geological process during early Paleozoic (Meng et al., 1997; Lee and Lee, 2003; Kwon et al., 2006). Chen et al (2012) compared the Cambrian Series 3 to Furongian succession between the Taebaeksan basin and the North China platform based on sequence stratigraphic and biostratigraphic data. However, sequence stratigraphic surfaces of Shangdong region of the North China Platform are rarely correlated with Taebaek region of the Taebaeksan basin because of 'the high variability of the bounding surface affected by a complex interplay among differential carbonate production, siliciclastic input, hydrodynamic conditions, and topographic relief (Chen et al., 2012).' This unsuitable correlation is due to lack of continuous outcrops of Taekback region. The focus of this study is application a new perspective mixed carbonate-siliciclastic model on The Sesong and Hwajeol formations (Taebaek area) and The Machari Formation (Yeongweol area) deposited in mixed carbonate-siliciclastic setting of Tebaeksan basin during Cambrian Series 3 to Furongian ; and it correlates with coeval strata of the Gushan and Chaomidian formations (Shangdong area). Sequence stratigraphic interpretation of stable epicratonic mixed carbonate-siliciclastic setting of this region provides insight into the interplay between carbonate productivity and siliciclastic sediment input and complexity of this setting differed from traditional models.

2. Geological settings

The North China Platform and Taebaeksan Basin developed on the Sino-Korean Block (SKB) deposited in intracratonic basin setting of the subtropical to tropical regions during Cambrian (Meng et al., 1997; Kwon et al., 2006; McKenzie et al., 2011). SKB is bounded to the north by the Hinggan fold belt (major suture zone) and the south by the Qinling-Dabieshan fold belt which contacts with the South China Block (SCB). According to the paleogeographic reconstruction and stratigraphic correlation, the Taebaeksan Basin comprises the eastern margin of the platform (Chough et al., 2000; Kwon et al., 2006).

The Joseon Supergroup of the Taebaeksan Basin is represented by lower Paleozoic sedimentary rocks interpreted to have formed in mixed siliciclastic-carbonate marine environments that are located in the mid-eastern part of the Korean peninsula (Fig. 1). The Joseon Supergroup unconformably overlies Precambrian granitic gneiss and meta sedimentary rocks and is unconformably overlain by the Carboniferous to Triassic Pyeongan Supergroup, and it can be divided into five lithologic units: Yeongwol, Taebaek, Yongtan, Pyeonchang, and Munyeong groups (Fig. 2-1A) (Choi, 1998). The Taebaek Group consists of 11 formations (about 1000-1400 m thick): the Jangsan/Myeonsan, Myobong, Daegi, Sesong, Hwajeol, Donjeom, Dumugol, Makgol, Jigunsan, and Duwibong formations, in ascending order (Kwon et al, 2006). The Yeongwol Group is exposed in the western part of the Taebaeksan Basin and is subdivided into the

Sambangsan, Machari, Wagok, Mungok, and Yeonheung formations, in ascending order.

The Cambrian strata of the North China Platform are well exposed in Shangdong Province. The Cambrian succession in Shangdong province is composed of six lithostratigraphic units: Liguan, Zhushadong, Mantou, Zhanxia, Gushan, and Chamonidian formations in ascending order, unconformably overlying Precambrian granitic gneiss or locally Late Proterozoic metasedimentary rocks, and conformably underlying Ordovician dolostones and limestones (Chough et al., 2010; Chen et al., 2011).

Trilobite biozones of Sesong and Hwajeol formations (Taebaek group) are composed of *Jiulongshania, Neodrepanura, Liostracina, Fenghuangella, Prochuangia, Chuangia, Kaolishania, Asioptychaspis, Quadraticephalus, Eosaukia* in ascending order. Trilobite biozones of Machari Formation (Yeongweol group) consist of *Tonkinella, Lejopyge armata, Glyptagnotus stolidotus, Gyptagnostus reticulatus, Proceratopyge tenuis, Hancrania brevilimbata, Eugonocare longifrons, Eochuangia hana, Agnostotes orientalis, Pseudourepingia asaphoides* in ascending order. Trilobite biozones of Gushan and Chaomidian formations are composed of *Blackwelderia, Neodrepanura, Chuangia, Changshania-Irvingella, Kaolishania, Asioptychaspis-Tsinania, Quadraticephalus* in ascending order (Fig. 2-2).

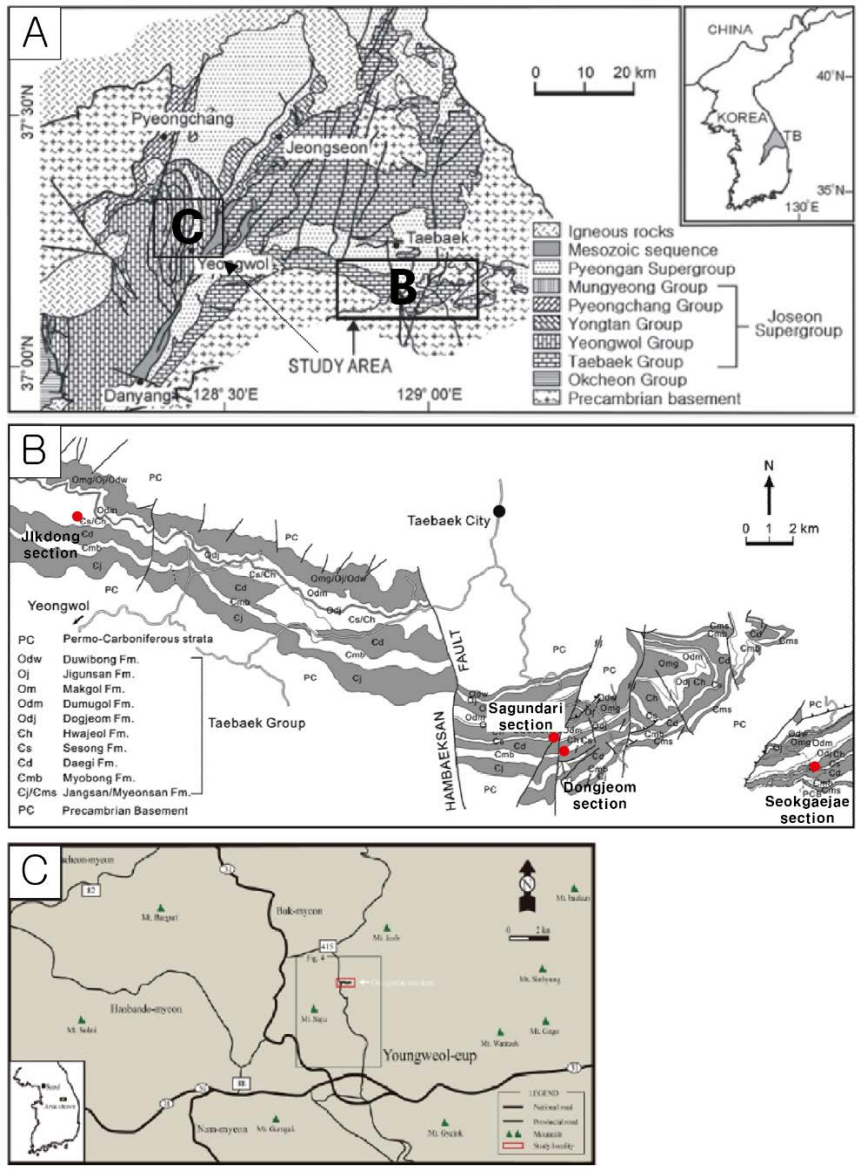

Fig. 2-1. (A) Simplified geologic map of Joseon Supergroup and the location of study area. (Modified from Kwon et al., 2006) (B) Geologic map of the Dongjeom section in the Taebaeks area. Modified from Jang and Choi (2007) (C) Index map of the Deogwoo section of the Yeongweol area (Choi and Ryu, 2013).

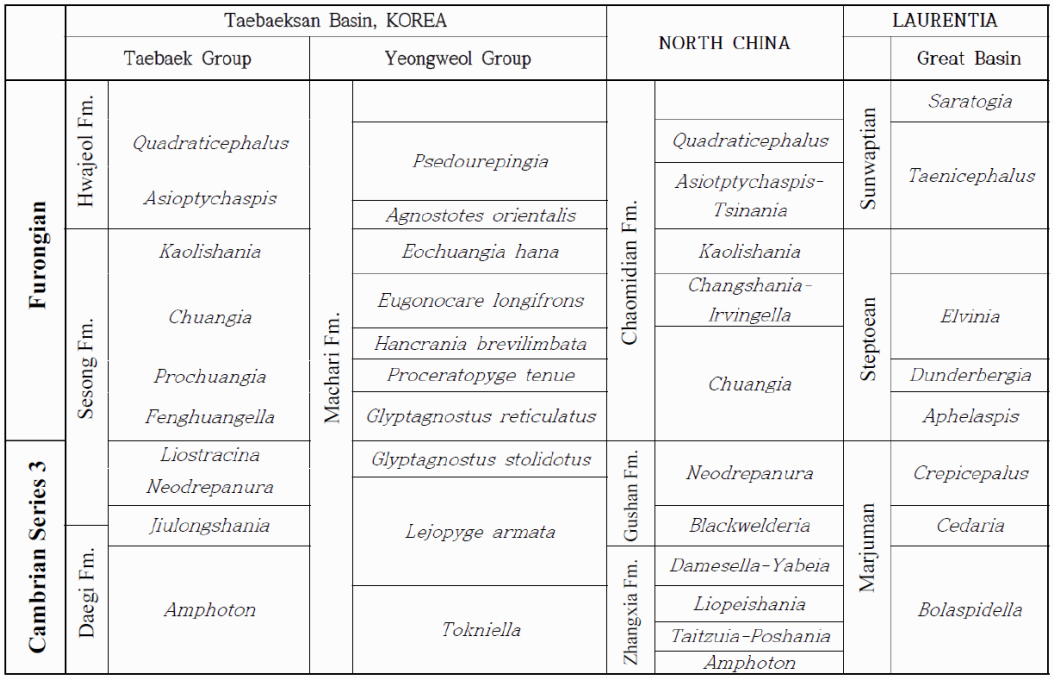

Fig. 2-2. Correlation of the Late Cambrian trilobite zones of the Sesong Formation and the Machari Formation with coeval global zones. Data from Taebaek (Sohn and Choi, 2007; Park and Choi, 2011; Park et al., 2012, 2013), Yeongweol (Lee and Choi, 1994, 1995; Choi and Lee, 1995; Hong et al., 2003), N. China (Meng et al., 1997; Chen et al., 2011) and North America (Palmer, 1990).

3. Method

3.1. Field work

The study area of the Seosong and Hwajeol formations (Dongjeom section) is located beside the railroad near the Dongjeom station (Fig. 2-1B). In the Dongjeom section, about 190 m outcrop succession was recorded in columnar section with photographs, and 61 rock samples of Seosong Formation (1-3 m interval) and 29 rock samples of Hwajeol Formation (3-5 m interval) are collected. In the Deogwoo section of the Machari Formation located along the valley (Fig. 2-1C), detailed sedimentary facies analysis and sequence stratigraphic research are conducted by Chung et al. (2011) and Choi and Ryu (2014). According to detailed columnar section (ca.190 m thick) recorded by Choi and Ryu (2014), 77 rock samples are collected at 1-5 m interval.

3.2. Insoluble residue

Insoluble residues are extracted from total 61 samples (15 samples in the Sesong and 46 samples in the Machari). The limestone, argillaceous limestone, calcareous mudstone and mudstone samples were cut into small chips by water-cooled saw, and the fresh chips containing no veins were picked out and ground into powder. 2-30 g samples were decarbonated by 2 N hydrochloric acid. The carbonate-free residues were first neutralized

by a stepwise centrifugation process and then dried at 75-85 °C and eventually weighed. Such a chemical process can remove most of the chemical precipitates in the sedimentary rocks, such as carbonates, Fe-Mn oxyhydroxides and absorbed materials except organic materials, sulfur and biogenic siliceous materials (Wei et al., 2003, 2006). This treatment can be well used to gain information about the composition of terrigenous detritus (Zhao et al., 2015).

3.3. Stable carbon isotope

40 samples of Sesong and Hwajeol formations were collected for stable carbon and oxygen isotope analysis. Rock samples such as sandstone, siltstone, and mudstone with carbonate were crushed and pulverized to powder in agate mortars for stable carbon and oxygen isotope analysis. Powder sampling spot considered at the least altered spot avoiding vein. The analysis of stable carbon and oxygen were conducted at the university of Michigan department of geological sciences stable isotope laboratory. The powdered samples were reacted with phosphoric acid in an online carbonate preparation line connected to a Finnigan Mat 251 mass spectrometer. The analytical precision of $\delta^{13}C_{carb}$ based on duplicate analysis and on multiple analysis of NBS19 was $\leq 0.04‰$.

3.4. Whole rock geochemistry

46 samples from Machari Formation and 15 samples from Sesong Formation were collected for analysis of whole rock geochemistry. Insoluble residues are extracted from 61 sample for removing carbonate fraction. 61 samples were geochemically analyzed for major, trace, and rare earth elements at Korean Basic Science Institute. Major element analysis was conducted using Philips PW 2404 X-ray fluorescence (XRF) spectrometer. Trace and rare earth element concentrations were obtained by Elan DRC Ⅱ Inductively Coupled Plasma Mass Spectrometer (ICP-MS) and OPTIMA 4300 DB Inductively Coupled Plasma-Atomic Emission Spectrometer (ICP-AES).

4. The Sesong and Hwajeol formations

4.1. Facies Association

The outcrops of the Sesong and Hwajeol formations of Taebaek area are distributed at Seokgaejae, Dongjeom, Sagundari, and Jikdong (Fig. 2-1A). Facies analysis and sequence stratigraphic interpretation of the Sesong and Hwajeol formations are conducted at Seokgaejae (Kwon et al., 2006), Dongjeom (Joo and Ryu, 2012), and Sagundari and Jikdong (Lim et al., 2015) sections. However, these works were carried out from limited discontinuous outcrops, thus, their interpretations had a limitation in sequence stratigraphic analysis. We analyzed sedimentary lithofacies of the Sesong and Hwajeol formations at a continuous outcrop of Dongjeom section with other sections (Fig. 2-1A). The Sesong and Hwajeol formations of Taebaek is composed of nine lithofacies (Table. 4-1), which are laminated mudstone (Ml), lime nodule-bearing shale (Sn), limestone-shale couplet (L-S), anastomosed wackestone to packstone (Wpa), laminated siltstone (Ls), laminated sandstone (Sl), massive sandstone (Sm), calcareous sandstone, and lime pebble conglomerate (Clp). These lithofacies were grouped into four facies association (Table. 4-2); carbonate and shale offshore association (FA1), Siliciclastic offshore (FA2), offshore transition FA3), and Shoreface association (FA4).

Fig. 4-1. Columnar sections of the Sesong and Hwajeol formations in the study area. Green line indicates trilobite biozone. Columnar section and tirilobite biozone of Jikdong modified after Park and Choi (2011) and Lim et al. (2015). Columnar section and trilobite biozone of Sagundari and Seokgaejae sections modified after Sohn and Choi, 2007; Park et al., 2013).

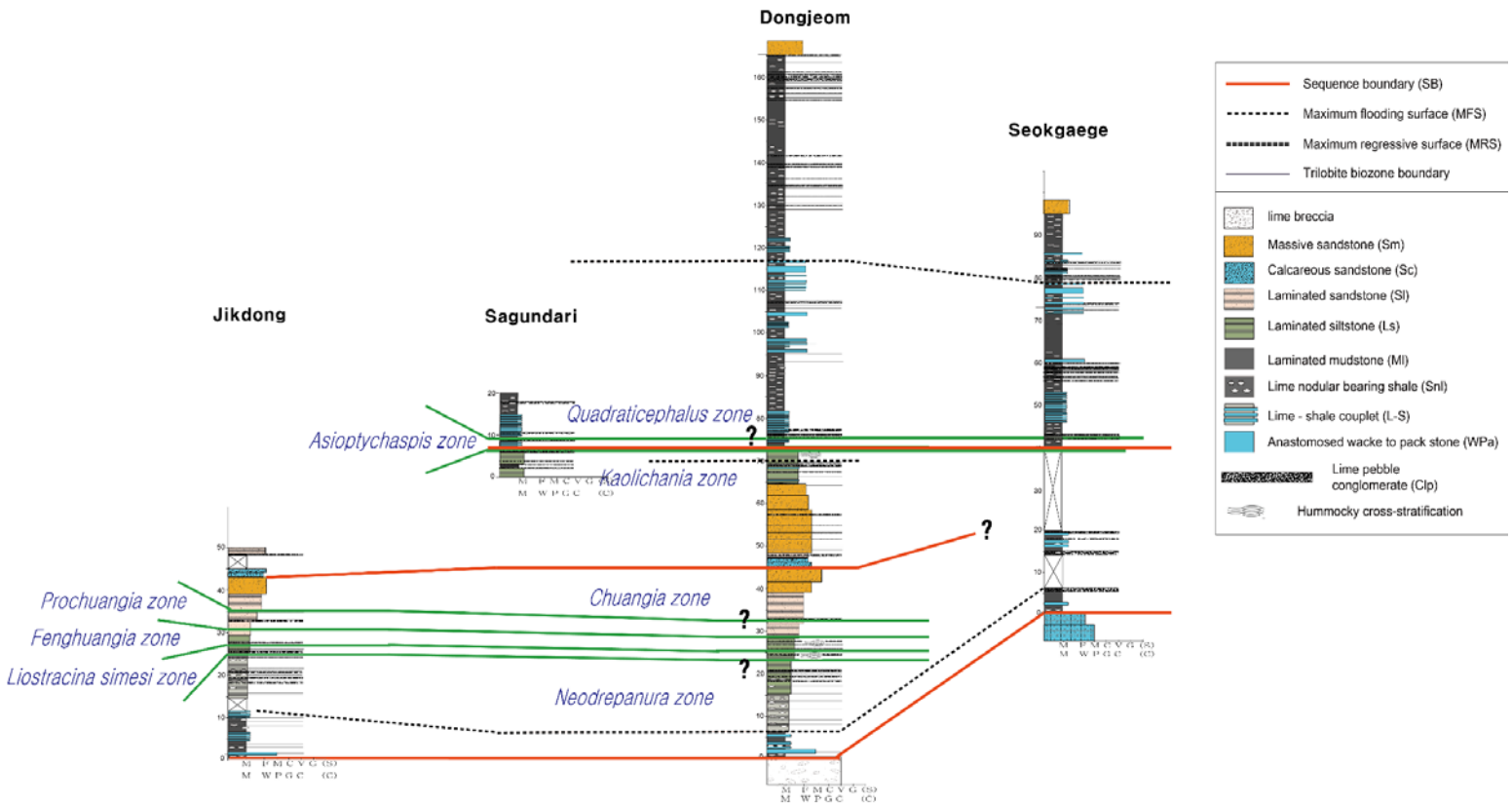
Dongjeom
Seokgaege
Jikdong
Sagundari
Quadraticephalus zone
Asioptychaspis zone
Kaolichania zone
Prochuangia zone
Fenghuangia zone
Liostracina simesi zone
Chuangia zone
Neodrepanura zone
?
Sequence boundary (SB)
Maximum flooding surface (MFS)
Maximum regressive surface (MRS)
Trilobite biozone boundary
lime breccia
Massive sandstone (Sm)
Calcareous sandstone (Sc)
Laminated sandstone (Sl)
Laminated siltstone (Ls)
Laminated mudstone (Ml)
Lime nodular bearing shale (Snl)
Lime - shale couplet (L-S)
Anastomosed wacke to pack stone (WPa)
Lime pebble conglomerate (Clp)
Hummocky cross-stratification

Table 4-1. Sedimentary facies of the Sesong and Hwajeol formations

Lithofacies	Description	Interpretation
Laminated mudstone (Ml)	Alteration of laminated terrigenous mud and calcareous mud. Silt-size sediments are occasionally included in boundaries between laminae. Sometimes, laminae of mudstone are faint; and it looks like black homogeneous mudstone (Fig. 4-2A).	Deposited from suspension fall out under low-energy condition and low-density turbidity current (Kwon et al., 2006)
Lime nodule-bearing shale (Sn)	The calcareous nodule is oval-shaped or elongated parallel to laminae, and it consists of calcareous mud or fossil fragment. The thickness of nodule ranges from 0.5cm to 3 cm. Terrigenous mud around nodule is light to dark gray. The boundary between nodule and mud is gradually or abruptly changed (Fig. 4-2B).	Deposited from suspension fall out under low-energy condition and, low-density turbidity current within early diagenesis (Wanless, 1979)

Laminated siltstone (Ls)	Alteration of green, gray, and dark-gray color; Normal grading with alteration of terrigenous silt and mud, and occasionally fine sand; It sometimes contains fossil fragments; It display small-scale hummocky cross-stratification (Fig. 4-2C).	Deposited during high-energy periods recorded as distal tempestites (Runkel et al., 1998; Labaj and Pratt., 2016)
Laminated sandstone (Sl)	Fine to medium sandstone alternate with dark gray mudstone and siltstone; parallel lamination with normal grading; occasional small-scale hummocky cross-stratification; differs from Laminated siltstone (Ls) in coarser grain size and proportion of mud (Fig. 4-2D).	Deposited by storm-, wave-, and tide-induced currents in shoreface (Runkel et al., 1998; Kwon et al., 2006)
Massive sandstone (Sm)	Fine to coarse sandstone intercalate with dark gray granular band; crudely stratified between light and dark color; dark gray sandstone	Deposited by strong currents and wave- and tide- induced currents; intermingled by

	represents nodule-like, patch like shape or poorly stratified with light colored sandstone (Fig. 4-2E).	bioturbation (Kwon et al., 2006)
Calcareous sandstone (Sc)	Light colored calcareous fine to medium sandstone intermingled with dark gray siltstone to fine sandstone; bioturbated (Fig. 4-2F)	Deposited by wave- and tide-induced currents; intermingled by bioturbation (Kwon et al., 2006)
Limestone-shale couplet (L-S)	Alteration of thick laminated (6~8 mm) to thin bedded (1~3 cm) light gray calcareous mud and dark gray terrigenous mud. Calcareous mudstone contains small portion of peloids and fossil fragments (Fig. 2G)	Deposited from suspension fall out under low-energy condition and, low-density turbidity current within early diagenesis or cyclic succession from environment change (Elrick et al., 1991, Badenas et al., 2012, Amberg et al., 2016)
Anastomosed wackestone to	Light gray to gray massive or nodule shape limestone; It consists	Deposited from subtidal and modification by

packstone (Wpa)	of lime mud and fossil fragments. Terrigenous silt to clay sized mud are distributed of irregular anastomosed shape (Fig. 4-2H).	compaction (Kwon et al., 2006)
Lime pebble conglomerate (Clp)	Lime pebble consists of rounded to subrounded, granule- to pebble-grade gravel clasts; it sometimes contains 1 to 20 cm long flat pebbles; lime clasts consists of laminated wackestone to grainstone clasts; subparallel to parallel to bedding plane, occasionally imbricated or edgewise structure; matrix of lime pebble conglomerate consists of micrite, peloids, fossil fragments; sharp erosional base; comparatively lateral extension, sometimes abrupt lateral change (Fig. 4-2I)	Deposited from storm sedimentation and autoconglomeration (Kwon et al., 2006; Chen et al., 2009)

.

Table 4-2. Facies associations of the Sesong and Hwajeol formations

Facies association	**Lithofacies**	**Depositional environment**
FA1	Laminated mudstone (Ml), Lime nodule-bearing shale (Sn), Limestone-shale couplet (L-S), Anastomosed wacke to packstone (Wpa), Lime pebble conglomerate (Clp)	Carbonate and shale offshore
FA2	Laminated mudstone (Ml), Laminated siltstone (Ls), Lime nodule-bearing shale (Sn), Laminated sandstone (Sl), Lime pebble conglomerate (Clp)	Siliciclastic offshore
FA3	Laminated siltstone (Ls), Laminated sandstone (Sl), Lime pebble conglomerate (Clp)	Offshore transition
FA4	Laminated sandstone (Sl), Massive sandstone (Sm), Calcareous sandstone (Sc), Lime pebble conglomerate (Clp)	Shoreface

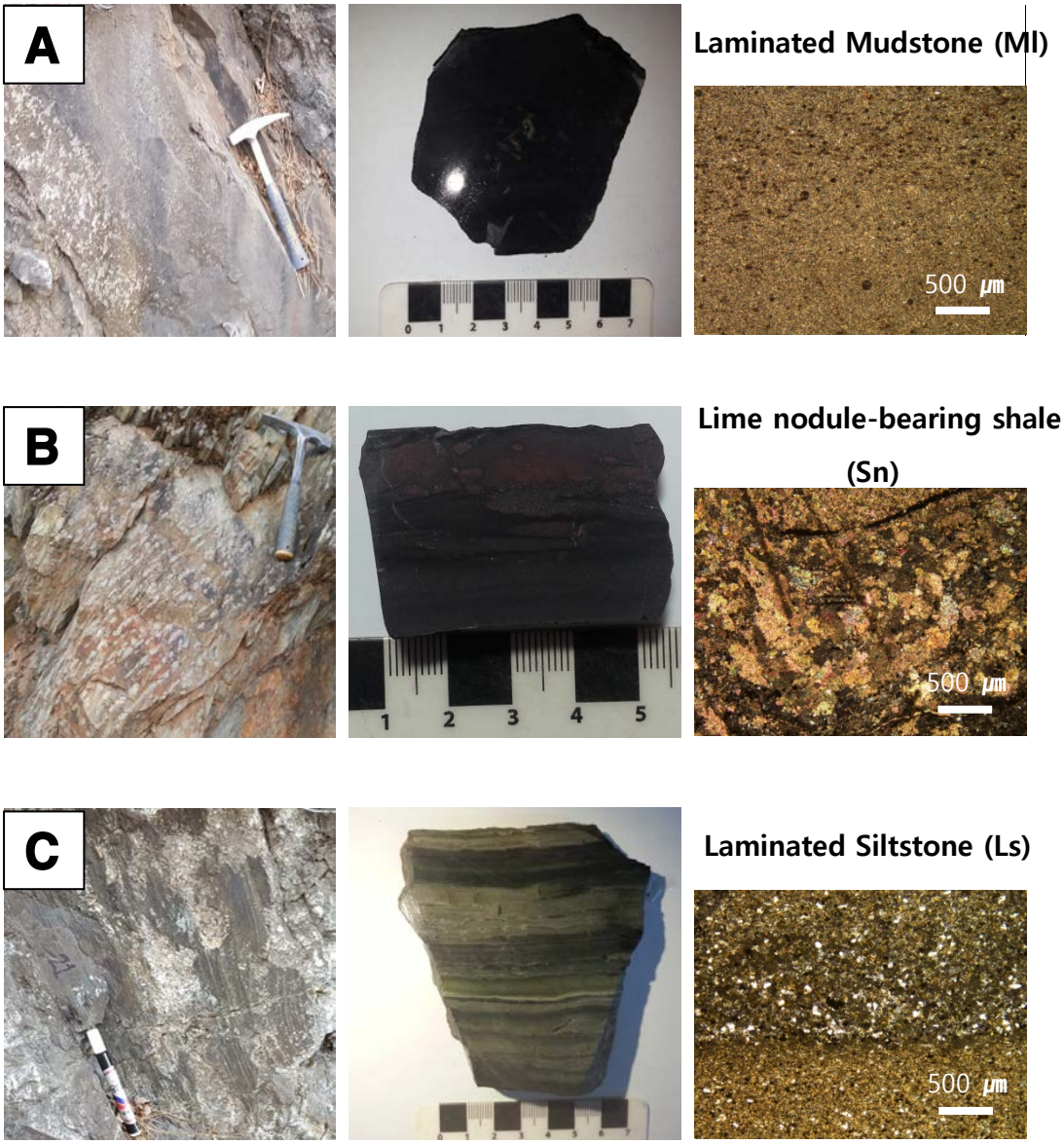

Fig. 4-2. Lithofacies of the Sesong and Hwajeol formations. From the left, photographs of outcrop, rock slab, and photomicrograph (hammer for scale is 27 cm long; pen for scale is 15 cm long). (A) Laminated mudstone (Ml), (B) lime nodule-bearing shale (Sn), (C)

Laminated siltstone (Ls).

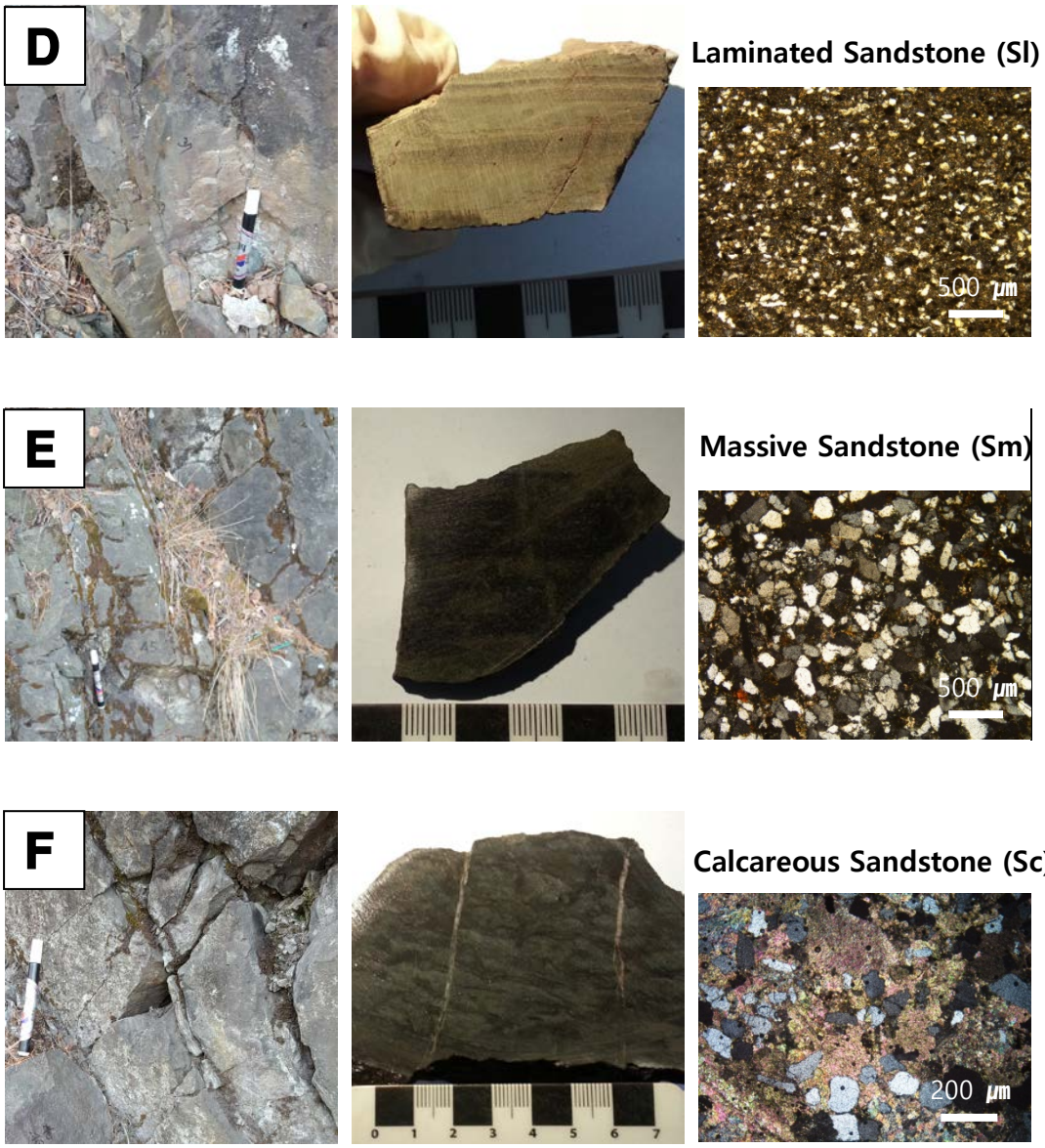

Fig. 4-2. Continued. (D) Laminated sandstone (Sl), (E) Massive sandstone (Sm), (F) Calcareous sandstone (Sc).

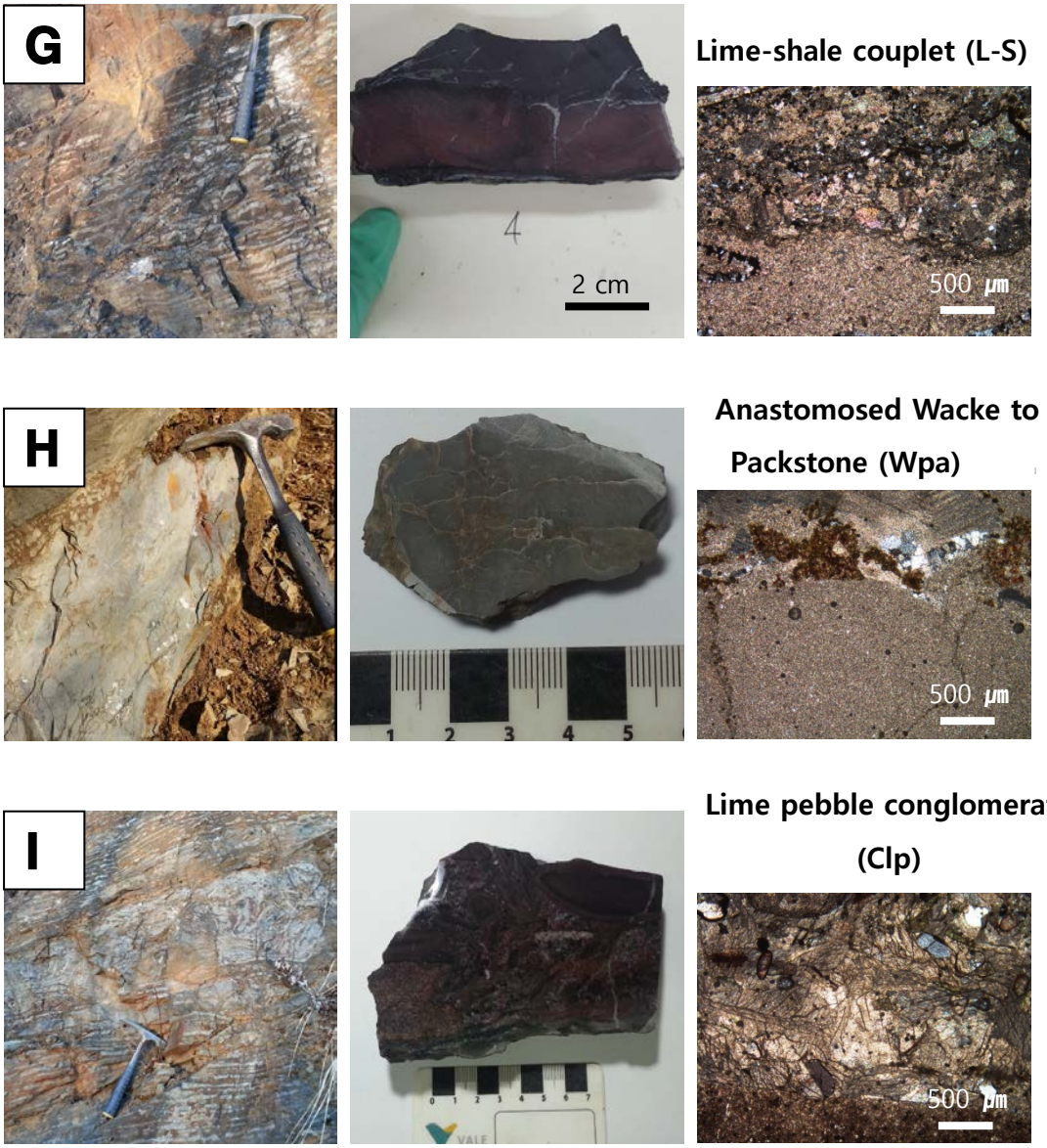

Fig. 4-2. Continued. (H) Anastomosed wackestone to packstone (Wpa), (I) Lime pebble conglomerate (Clp).

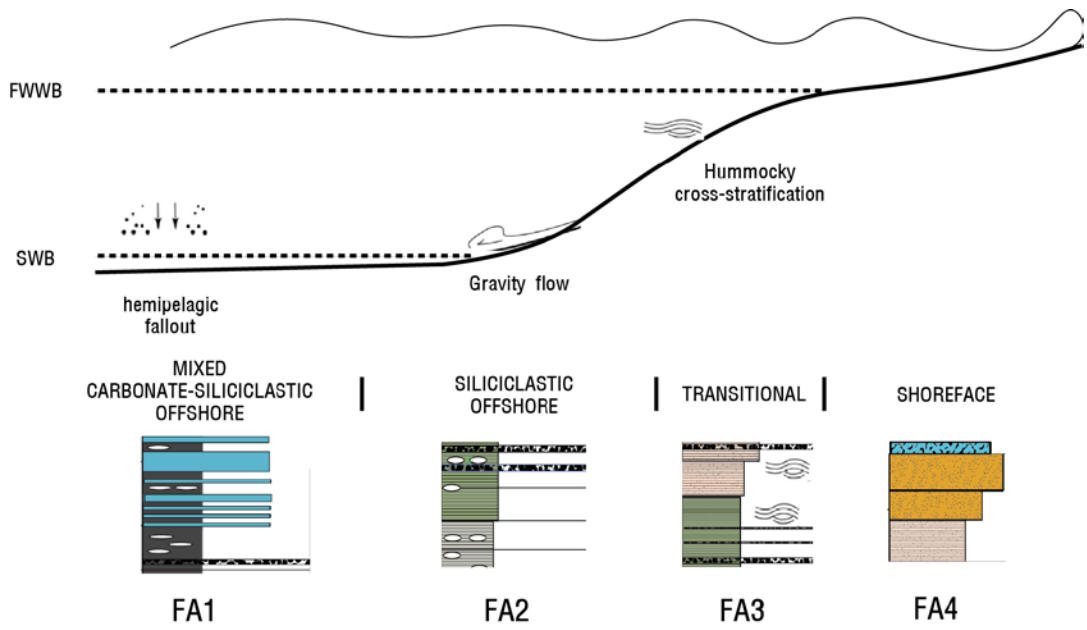

Fig. 4-3. Depositional model of the Sesong and Hwajeol formations. Diagram summarizing idealize stratigraphic sections of facies associations with their distribution on the bathymetric profile.

4.1.1. FA1: Carbonate and shale offshore association

FA1 consists of laminated mudstone (Ml), lime nodule-bearing shale (Sn), limestone-shale couplet (L-S), anastomosed wacke to packstone (Wpa), and lime pebble conglomerate (Clp) (Fig. 4-3; Table. 4-2). Lime mud and terrigenous mud were deposited from suspended fall out under low-energy condition and dilute turbidity current. Lime mud derived from water column and plume from the close carbonate-producing area. The source of terrigenous mud was riverine flume after storm or fluvial discharge as low-density clouds or plume of suspended sediment (Osleger and Read, 1991; Labaj and Pratt, 2016). Lime nodule-bearing shale was also deposited by suspended fall and low-density turbidity current with early diagenesis. The origin of limestone-shale couplet is enigmatic; one hypothesis is cyclic change of environment, whereas another is diagenetic perspective (Elrick et al., 1991; Badenas et al., 2012; Amberg et al., 2016). In any case, depositional environment of limestone-shale couplet was low energy environment influenced by occasional storm activity. Anastomosed wacke to packstone was deposited from subtidal zone and modified by compaction. Lime pebble conglomerate represents storm-induced facies. FA1 is interpreted as having been deposited just below the storm wave base in the offshore setting influenced by both of terrigenous and carbonate input with occasional storm activity.

FA1 occurs in the lower part of the Sesong Formation and lower and middle part of the Hwajeol Formation (Fig. 4-1) This facies association represents cyclic succession which consists of five lithofacies; laminated mudstone, lime nodule-bearing shale, lime-shale

couplet, anastomosed wacke to packstone, and lime pebble conglomerate in ascending order. In this cycle, Shale dominated lithofacies gradually changes into upward-thickening limestone lithofacies from laminated mudstone to anastomosed wacke to packstone. The top of cycle capped by lime pebble conglomerate with abrupt erosional base. Lime pebble conglomerate was deposited from early cemented lime mudstone by storm reworking. Otherwise, lime pebble and fossil fragment of matrix were transported from near carbonate producing area by scouring and reworking of storm current. This cyclic succession was interpreted by shallowing upward subtidal cycle in the Taebaek area (Ryu et al., 2005; Kwon et al., 2006; Woo et al., 2007). However, Myrow et al (2012) interpreted this cycle as deepening upward cycle; upward increasing-carbonate and decreasing of shale percentage represents increasing degree of condensation and decline of siliciclastic mud. Lime pebble conglomerate, which is the cap of cycle, was deposited by widespread cementation and increased storm intensity by maximum transgression (Myrow et al., 2012). There are also pebbles with stained outer rims (brown to purple color) within lime pebble conglomerate in the upper part of the Hwajeol Formation (Joo and Ryu, 2011). This stained pebble seems to be ferromanganese crusts which are produced by long-term exposure to the seawater; and it indicates environment with extremely low sediment accumulation rate (Follmi et al., 2016). Stained ferromanganese pebble supports deepening upward cycle (i.e. lime pebble conglomerate indicates condensed section). In this cycle of FA1, there occasionally are absence of components of full cycle; lime pebble conglomerate, for example, is not exist in middle part of the Hwajeol Formation. This lack of cycle components was due to relative controls of carbonate input, siliciclastic input, relative sea-

level change, and degree of reworking.

4.1.2. FA2: Siliciclastic offshore association

FA2 is composed of laminated mudstone (Ml), laminated siltstone (Ls), lime nodule-bearing shale (Sn), laminated sandstone (Sl), lime pebble conglomerate (Clp) (Fig. 4-3; Table 4-2). Compared to FA1, FA2 mainly consists of lime nodule bearing shale, laminated mudstone, and laminated siltstone; and proportion of carbonate was decreased (e.g., lack of anastomosed wacke to packstone and decrease of lime-shale couplet lithofacies). Also, laminated mudstone and siltstone of FA2 commonly represent normal grading. Silt-size quartz grains is concentrated in boundaries between lamination. Laminated or structureless siltstone beds grading upward into mudstone. Graded beds deposited by wave action during extreme storm events (Runkel et al., 1998). Silt is probably transported by sediment plumes, which is generated by drainage after storm surges, or fluvial discharge which then moved into offshore as dilute clouds or plumes of suspended sediment (Osleger and Read, 1991; Labaj and Pratt, 2016). Lime pebble conglomerate deposited by storm reworking. Rounded intraclasts of lime pebble conglomerate indicate repeated storm reworking. FA2 occurs in the lower and upper parts of the Sesong and Hwajeol formations. FA2 is interpreted as having been deposited above the storm wave base in the offshore setting, but FA2 was more influenced by siliciclastic input than FA1.

4.1.3. FA3: Offshore transition association

FA3 is composed of laminated siltstone (Ls), laminated sandstone (Sl), lime pebble conglomerate (Clp) (Fig. 4-3; Table 4-2). Compared to FA2, FA3 mainly consists of sandstone facies and distinctively includes hummocky cross-stratification (HCS). FA3 was deposited by suspension fallout during calm condition, alternating with the influences of storms that transported sand from nearshore and reworked it by oscillatory currents (Labaj and Pratt, 2016). HCS of sandstone beds indicates strong storm events. HCS was formed by combination of unidirectional and oscillatory flows. The predominance of HCS indicates that large-scale storms frequently influenced the transitional environment (Eoff et al., 2014b). HCS could mostly have formed in marine environment above storm wave base and below fairweather wave base, because the preservation potential of HCS is decreased above fairweather wave base (Dott and Bourgeois, 1982; Eoff et al., 2014b). Lime pebble conglomerate more frequently present in FA3 than that of FA2. The thickness of lime pebble conglomerate also increases in FA3. The common occurrence of Lime pebble conglomerate implies that FA3 was more influenced by storm reworking than FA2. FA3 is interpreted to have been deposited between storm wave base and fairweather wave base and influenced by frequent storm activity.

4.1.4. FA4: Shoreface association

FA4 consists of laminated sandstone (Sl), massive sandstone (Sm), calcareous sandstone (Sc), lime pebble conglomerate (Clp) (Fig. 4-3; Table 4-2). Massive and laminated sandstones predominantly occur in FA4, locally with calcareous sandstone and lime pebble conglomerate. Massive sandstone is deposition from rapid suspension settling and indicative of high accumulation rate (Kwon et al, 2006). Crudely stratification which is formed by strong currents occasionally represents in massive sandstone. Laminated sandstone is shoreface deposition formed by wave and current (Kwon et al., 2006). Massive sandstone is composed of mostly quartz grain, occasionally with feldspar and rock fragment. According to Joo and Ryu (2012), fine to medium grained sandstone in Sesong Formation of Dongjeom section is interpreted as quartzose wacke based on modal analysis. Quartzose wacke was commonly deposited transitional continental, and fine to medium grained sandstone is deposited in shoreface (Joo and Ryu, 2012). The cement of massive sandstone is mostly silica cement, partly with calcite cement. Massive sandstone shows long or sutured contact with quartz overgrowth (Fig. 4-5A). Calcareous sandstone shows floating grains or tangential contact in calcite cement and contains bioclasts (Fig. 4-5B). Calcite cement is commonly derived from biogenic carbonate which is contained within the sandstone (Kim and Lee, 2004). FA4 is interpreted to have been deposited in shoreface above fairweather base.

4.2 Depositional model

The depositional environment of the Sesong Formation was reported to be carbonate outer shelf (Kwon et al., 2006), clastic outer shelf (Choi, 2011), outer to inner shelf during relative sea-level fall (Joo and Ryu, 2012). Based on facies analysis at continuous outcrop of the Dongjeom section, mixed carbonate-siliciclastic Sesong and Hwajeol formations were deposited in nearshore settings of cratonic interior and influenced by storm activity including hummocky cross-stratification and flat pebble conglomerate (Fig. 4-3). Diverse carbonate facies interbedding with shale indicate warm and shallow-water settings and low paleolatitude (Lee and Lee, 2003). Carbonate production was interrupted by episodic terrigenous input. Carbonate facies of Seosong and Hwajeol formations are deposited just above or below storm wave base and more distal than siliciclastic facies. Thus, siliciclastic mud and sand were deposited in proximal detrital belt, and carbonate produced in distal carbonate belt. The facies of Sesong and Hwajeol formations are highly similar to those of inner detrital belt of Laurentia situating between a cartonic hinterland and a distal carbonate belt (Runkel et al., 1998, 2007; Myrow et al. 2012).

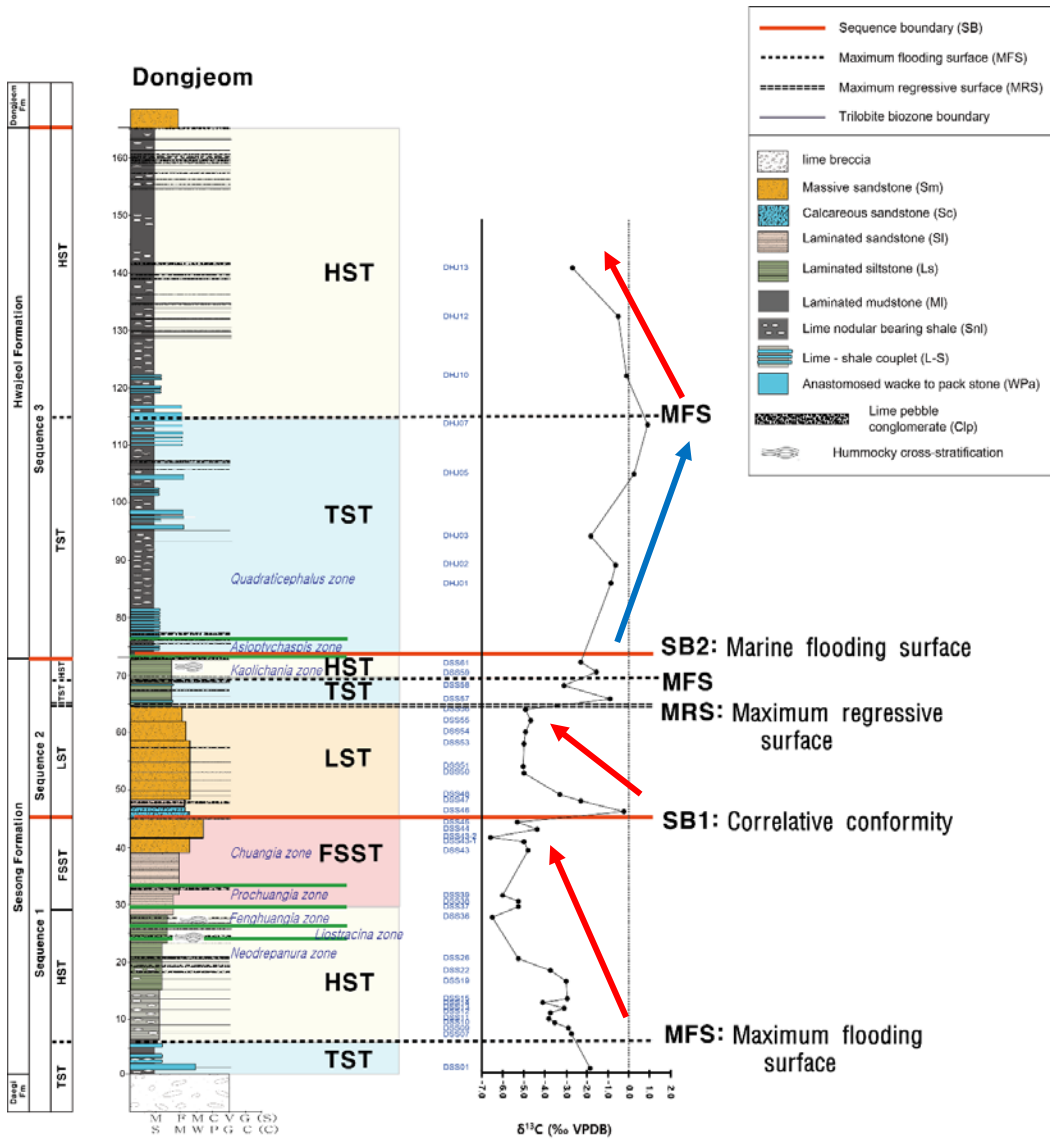

Fig. 4-4. Columnar section of Sesong and Hwajeol formations at the Dongjeom section showing biostratigraphy, sequence stratigraphy, and stable carbon isotope values. Red arrow means regressive phase and blue arrow indicates transgressive phase.

4.3 Sequence stratigraphy

Based on facies analysis, Seosong and Hwajeol formations are composed of four facies association; carbonate and shale offshore association (FA1), Siliciclastic offshore (FA2), offshore transition (FA3), and Shoreface association (FA4). These more or less contemporaneous facies associations were laterally migrated and deposited in the mixed carbonate-siliciclastic environment in response to eustasy, subsidence, carbonate production, and siliciclastic sediment input. Systems tract generally indicate contemporaneous depositional systems and characterized by their internal geometry (Van Wagoner et al., 1990; Catuaneanu, 2006). A sequence contains a falling stage systems tract (FSST), a lowstand systems tract (LST), a transgressive systems tract (TST), and a highstand systems tract (HST) (Catunuanu, 2006).

4.3.1. Sequence 1

The mixed carbonate-siliciclastic succession of Sesong and Hwajeol formations consists of three sequences (Fig. 4-4). The base of the Sesong formation record TST which represent carbonate and shale offshore facies association without lowstand deposits, underlain by the shallow carbonate facies of Daegi formation. This boundary is defined as Type-3 sequence boundary between supersequence Ⅰ and supersequence Ⅱ by Kwon et al (2006). They concluded that entire Sesong Formation is transgression base on upward decrease in frequency and thickness of interbedded limestone layers (Kwon et al., 2006).

However, upward decrease carbonate facies is caused by interruption of siliciclastic input to the carbonate factory. The amount of silt- and sand-sized sediments also increase with changing from FA1 to FA2. This boundary changing from FA2 to FA1 is a maximum flooding surface (MFS). FA1 is dominated by wacke to packstone, lime-shale couplet, lime nodule-bearing shale, and homogeneous shale which are deposited under stable condition below storm wave base interbedded by occasional lime pebble conglomerate. Beginning with HST, laminated siltstone and laminated sandstone, which represents normal grading formed by storm-induced gravity flow, were deposited, and coarsening-upward interval starts with aggradational and progradational stacking. FA2 gradually change to FA3 with storm-induced hummocky cross-stratification and lime pebble conglomerate.

HST is terminated by following FSST which consists massive sandstone and laminated sandstone occasionally with lime pebble conglomerate (Fig. 4-6A). Compared to HST, FSST is dominantly composed of medium to coarse-grained massive sandstone which is deposited by rapid suspension settling (Fig. 4-6C). Sandstones of FSST also show long or sutured contact with quartz overgrowth which means rapid deposition and compaction formed in regressive phase (Fig. 4-5A). With relative sea-level fall, siliciclastic was dominantly deposited with feldspars breaking into small pieces by reworking. Thus, quartzose wacke were deposited and experienced physical compaction with little calcite cementation in the early diagenesis and chemical compaction with quartz cementation in the late diagenesis (Kim and Lee, 2004). Subsequently, coarse grained massive sandstone abruptly changed to fine to medium grained calcareous sandstone. The surface

transitioning from non-calcareous sandstone to calcareous sandstone is sequence boundary (SB1) between sequence 1 and sequence 2 (Fig. 4-6B). SB1 is correlative conformity, which lacks clear evidence for subaerial exposure such as significant erosion and paleosols. SB1 are nearly flat because of steady, prolonged eustatic fall across the low-relief stable cratonic interior which has less complex sequence boundary than those formed in tectonically active settings (Runkel et al., 2007; Eoff et al, 2014). SB1 possibly located between trilobite biozone *Chuangia* and *Kaolichania* in the Donjeom section which can be correlated with Jikdong and Sagundari section based on sequence stratigraphic analysis. *Chuangia* trilobite biozone can be biostratigraphically correlated with *Dunderbergia* trilobite biozone in Laurentia (Fig. 2-2, Park et al., 2013). SB1 corresponded to the Sauk Ⅱ-Sauk Ⅲ hiatus which associated with "sheet sandstone" (i.e., Wonewoc Formation of UMV; uppermost part of the Abrigo Formation of southwestern Arizona; Runkel et al., 1998, 2007; Labaj and Pratt, 2016). In middle-upper Cambrian, evidences indicating relative sea-level fall were globally reported such as South China (Peng et al., 2001), North China (Chen et al., 2001), Kazakhstan and Austrailia (Saltzman et al., 1998, 2000), North America (Saltzman et al., 1998; Glumac and Spivak-Brindorf, 2002), and Spain and France (Alvaro et al., 2007).

4.3.2. Sequence 2

Above SB1, LST was deposited representing coarsening-upward progradational to aggradational trends (Fig. 4-4). Rising of base-level started after formation of correlative conformity, but the creation of accommodation was still diminished. When the dominant depositional trend changed from progradational to aggradational, it is typically lowstand normal regression (Catuneanu et al., 2009). LST above the Sauk Ⅱ-Sauk Ⅲ hiatus in Laurentia also observed in upper part of Wonewoc Formation and overlain by TST which represents condensed section (Eoff et al., 2014b). TST of the upper part of the Sesong Formation at Dongjeom section also shows condensed features above MRS (Fig.4-7A). Although condensed section are not confined in maximum flooding interval, the majority of condensed sections would have been formed during maximum intervals with sediment starvation (Van Wagoner et al., 1990; Eoff et al., 2014a). Sediment starvation during transgression with increasing of carbonate production resulted in the formation of calcareous cement, authigenic mineral and carbonate lags (Fig 4-7C). Abundant lime pebble conglomerate with abruptly changing in grain size indicate condensed section. Initiating TST, Non-calcareous massive sandstone facies of LST suddenly changes to calcareous fine sandstone. The grain size of sandstone also abruptly changes from medium sandstone to fine sandstone with increasing lime pebble conglomerate and lime nodule. Carbonate production increased during siliciclastic sediment starvation, it resulted in the formation of calcareous fine sandstone and lime pebble conglomerate which recorded by continued ravinement (Eoff et al., 2014a). TST is terminated by laminated fine sandstone

of HST with HCS (Fig. 4-7A). Laminated fine sandstone consists of quartz, feldspar, and muscovite mica (Fig. 4-7B). The presence of immature grains indicates proximity to source areas.

4.3.3. Sequence 3

Laminated fine sandstone is abruptly ended by limestone-shale couplet at the boundary between Sesong Formation and Hwajeol Formation, this boundary is SB2 formed by a rapid base-level rise (Fig. 4-4). Hwajeol Formation is dominated by FA1 which is composed of laminated mudstone (Ml), lime nodule-bearing shale (Sn), limestone-shale couplet (L-S), anastomosed wacke to packstone (Wpa), and lime pebble conglomerate (Clp). Facies of Hwajeol Formation gradually changes from L-S and Sn facies of lower part to Wpa and Sn facies of middle part with increasing carbonate proportion caused by TST. Base-level rise migrated shoreline to the landward and reduced terrigenous sediment supply. MFS is distinctively represented by a rapid change from Wpa, Sn, and Clp facies to Ml, L-S, and Sn facies. Above MFS, contents of carbonate gradually decreases caused by base-level fall starting with increasing terrigenous sediment. HST from the middle part to upper part is dominated by siliciclastic mud and continues to sandstone dominated Dongjeom Formation.

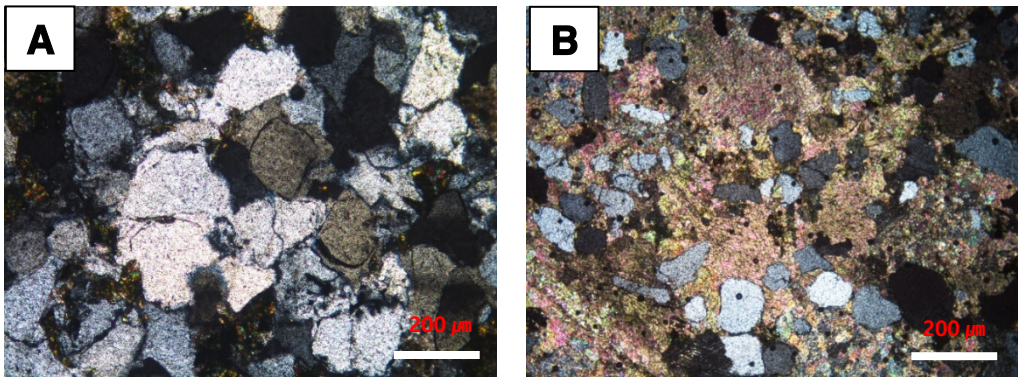

Fig. 4-5. (A) Photomicrograph of massive sandstone and quartz overgrowth (DSS 53 sample) (B) Photomicirohraph of calcareous sandstone (DSS 52 sample)

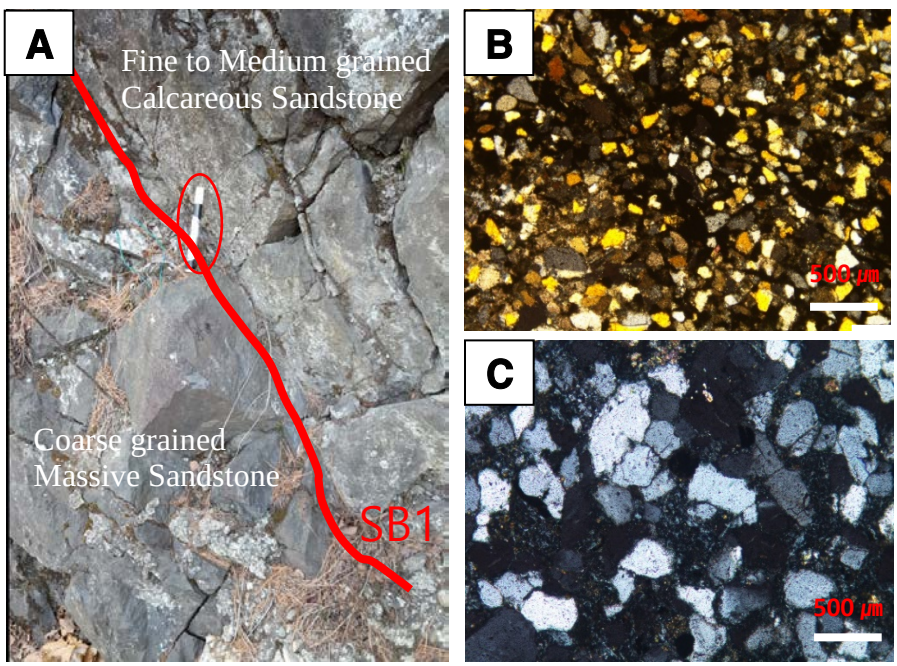

Fig. 4-6. (A) Outcrop photograph of SB1 with abrupt change from coarse grained massive sandstone to fine to medium grained calcareous sandstone in the middle part of the Sesong Formtion (pen for scale is 15 cm long). (B) Photomicrograph of fine to medium grained

calcareous sandstone (DSS46 sample). (C) Photomicrograph of coarse grained massive sandstone (DSS 44 sample).

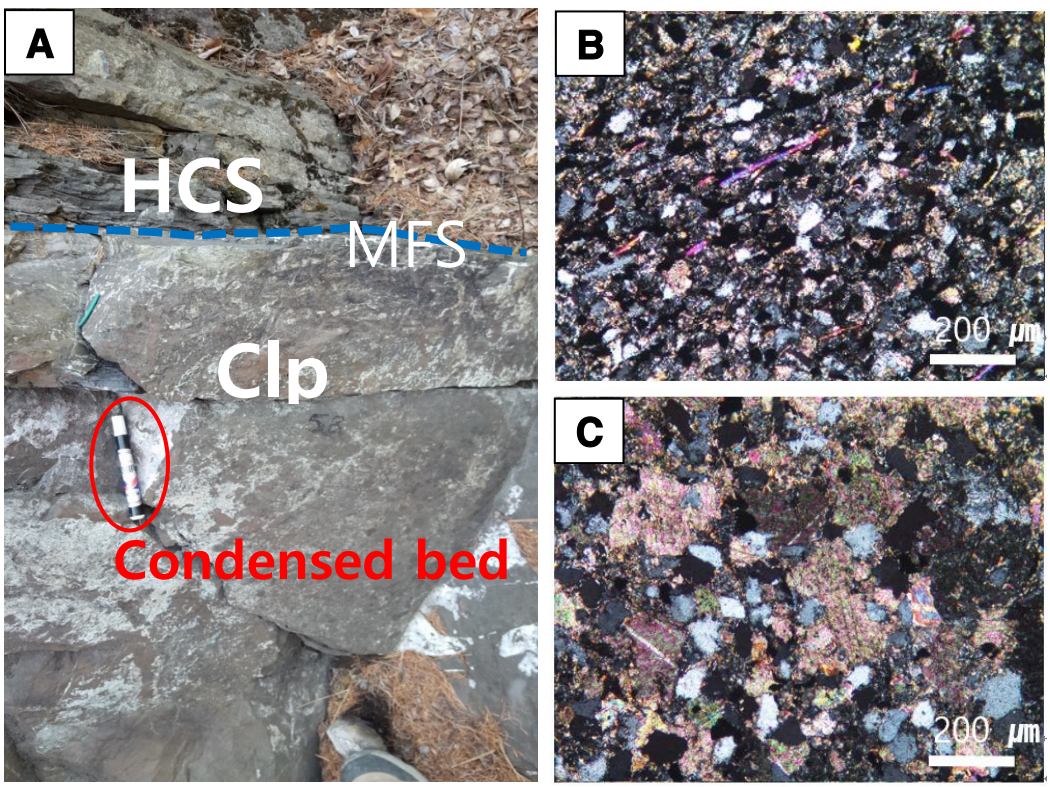

Fig. 4-7. (A) Outcrop photograph of MFS in sequence 2 with abrupt change from medium grained calcareous sandstone to fine grained laminated sandstone in the upper part of the Sesong Formtion (pen for scale is 15 cm long). (B) Photomicrograph of fine grained laminated sandstone which is composed of quartz, feldspar, and muscovite mica (C) Photomicrograph of fine to medium grained calcareous sandstone.

4.4. Stable Carbon Isotope

$\delta^{13}C_{carb}$ values range from -7 to 1‰ with two abrupt shifts at SB1 and MRS of sequence 2. $\delta^{13}C_{carb}$ values of Sesong and Hwajeol formations are largely divided into four sections (Fig. 4-4). The first section of $\delta^{13}C_{carb}$ values gradually decrease from -2 ‰ at the bottom of the Sesong Formation to -7 ‰ at the upper part of sequence 1. $\delta^{13}C_{carb}$ value abruptly shifts from -5 ‰ to 0 ‰ at SB1. Subsequently, $\delta^{13}C_{carb}$ value gradually decreases from 0 ‰ to -5 ‰, and maintains -5 ‰ until MRS of sequence 1 (second section). $\delta^{13}C_{carb}$ value drastically shift from -5 ‰ to -1 ‰ at MRS, and third section ranges -3 ‰ to -1 ‰. In last fourth section of Hwajeol Formation, $\delta^{13}C_{carb}$ value gradually increases from -2 ‰ of SB2 to 1 ‰ of MFS and subsequently decreases upward until -3 ‰.

Stable carbon isotope is generally used in chemostratigraphy by correlation with global carbon isotope excursion. However, $\delta^{13}C_{carb}$ values of whole rock sample have to consider carefully whether the $\delta^{13}C_{carb}$ values of sample record primary signals of ancient seawater or whether they were altered by diagenesis. During early diagenesis, $\delta^{13}C_{carb}$ values are mainly altered by the influence of meteoric water and remineralized organic carbon. Land plants did not influence considerably on the carbon cycle during the Cambrian. Thus, remineralized organic carbon derived from reworked marine sediments (Buggisch et al., 2003). $\delta^{13}C_{carb}$ values of subtidal carbonate are suitable for primary marine signals, but those of intertidal and supratidal carbonate are possibly altered by diagenesis. A big scatter of data and erratic changes of $\delta^{13}C_{carb}$ values also indicate diagenetic overprint. Meteoric water can influence several meters below emersion surfaces during eustatic sea-level falls

and lowstands (Buggisch et al., 2003). $\delta^{13}C_{carb}$ values of Sesong and Hwajeol formations show a big scatter and erratic changes, which it is altered by meteoric water. $\delta^{13}C_{carb}$ values of lower two sections show gradual decline and sharply termination by positive value. Gradual decline and maintain negative of $\delta^{13}C_{carb}$ values indicate that progradation and aggradation occurred when sedimentation rates outpace the low rates of base-level rise (normal regression) and the shoreline is forced to regress by base-level fall irrespective of sediment supply (forced regression) (Catuneanu, 2006). $\delta^{13}C_{carb}$ values well correlate with facies association, more calcareous offshore settings has more positive $\delta^{13}C_{carb}$ values. In the Hwajeol Formation, $\delta^{13}C_{carb}$ values gradually increase in TST and gradually decrease in HST. Our sequence stratigraphic interpretation is well matched with trends of $\delta^{13}C_{carb}$ values.

Late Cambrian (Furongian) mixed siliciclastic-carbonate and carbonate successions in many parts of the world contain an interval of markedly ~3‰–5‰ positive carbon isotope ($\delta^{13}C_{carb}$) excursions, which is termed the Steptoean Positive Carbon Isotope Excursion (SPICE) (Saltzman et al., 1998, 2000, 2004; Zhu et al., 2004; Kouchinsky et al., 2008; Ahlberg et al., 2009; Chen et al., 2011; Woods et al., 2011). Several geological events occurred in association with SPICE, including positive sulfur isotope excursion (Gill et al., 2011), a decrease in Mo isotope and concentrations (Gill et al., 2011), a long-term sea-level fall (Saltzman et al., 2004), mass extinction and faunal turnover of trilobites (Pratt, 1998; Saltzman et al., 2000; Peng et al., 2004, 2012; Álvaro et al., 2013), and reef transition with diversification of new organisms (Lee et al., 2015). SPICE interval in the Taebaeksan

basin of the Korean peninsula is recognized in the Machari Formation (Yeongwol area) by Chung et al. (2011) and the Sesong Formation (Taebaek area) by Lim et al. (2015). Lim et al. (2015) postulated SPICE at the lower part of the Paibian stage at Jikdong section. The peak of SPICE is coincided with a correlative conformity which corresponds to initiation of quartz sand influx (Lim et al., 2015). However, this correlative conformity is not well suggested, the boundary between laminated shale and massive sandstone is possibly boundary between HST and FSST. During forced regression, siliciclastic sediment input is largely increased, thus, massive sandstone facies was deposited. Based on stable carbon and oxygen isotope data of Lim et al. (2015), $\delta^{13}C_{carb}$ versus $\delta^{18}O_{carb}$ cross-plot shows a linear trend of the data point ($R^2 = 0.6042$) which infers to diagenetic overprint.

Table 4-3. Stable carbon and oxygen isotopes values of the Sesong and Hwajeol formations at the Dongjeom section.

sample	$\delta^{13}C_{carb}$ (VPDB)	$\delta^{18}O_{carb}$ (VPDB)	sample	$\delta^{13}C_{carb}$ (VPDB)	$\delta^{18}O_{carb}$ (VPDB)
DSS-1	-1.85	-17.91	DSS-46	-0.26	-23.54
DSS-7	-2.74	-24.10	DSS-47	-2.26	-22.31
DSS-9	-2.85	-19.66	DSS-48	-3.27	-21.73
DSS-10	-3.53	-20.51	DSS-50	-4.99	-22.96
DSS-11	-3.79	-22.64	DSS-51	-5.04	-19.65
DSS-12	-3.74	-22.51	DSS-53	-4.98	-24.57
DSS-13	-3.08	-24.01	DSS-54	-4.93	-24.16
DSS-14	-4.10	-24.22	DSS-55	-4.66	-23.02
DSS-15	-2.95	-24.20	DSS-56	-4.92	-22.61
DSS-19	-2.97	-24.30	DSS-57	-0.87	-22.73
DSS-22	-3.74	-24.04	DSS-58	-3.06	-22.42
DSS-26	-5.28	-23.44	DSS-59	-1.56	-22.45
DSS-36	-6.49	-23.07	DSS-61	-2.29	-22.61
DSS-37	-5.24	-22.05	DHJ-1	-0.85	-16.92
DSS-37-1	-5.26	-23.54	DHJ-2	-0.60	-16.38
DSS-39	-5.99	-21.53	DHJ-3	-1.78	-17.65
DSS-43	-4.79	-23.46	DHJ-5	0.27	-12.69
DSS-43-1	-4.97	-23.61	DHJ-7	0.91	-12.21
DSS-43-2	-6.59	-22.24	DHJ-10	-0.07	-14.41
DSS-44	-4.38	-24.16	DHJ-12	-0.49	-13.15
DSS-45	-5.31	-24.08	DHJ-13	-2.64	-18.33

5. Machari Formation

5.1. Facies association

The Machari Formation exposed at Deogwoo section located along the valley (Fig. 2-1C). Detailed sedimentary facies analysis and sequence stratigraphic research are conducted by Chung et al. (2011) and Choi and Ryu (2014). According to detailed columnar section (ca.190 m thick) and facies analysis recorded by Choi and Ryu (2014), we reinterpreted sequence stratigraphic framework based on new perspective models in the mixed carbonate-siliciclastic environment. Machari Formation consists of six lithofacies; black shale (Bs), laminated lime-shale couplet (Lls), bedded lime-shale couplet (Bls), lime nodule-bearing shale (Sn), anastomosed wackestone to packstone (Wpa), massive grainstone (Gm). These lithofacies are grouped into three facies association (Fig. 5-1; Table 5-1).

FA1 consists of black shale (Bs), laminated lime-shale couplet (Lls), bedded lime-shale couplet (Bls), lime nodule-bearing shale (Sn), and massive grainstone (Gm). Carbonate contents gradually increase from the bottom of the cycles and Gm caps the cycle (Table 5-2). Gm shows several condensed features such as hardground and pyrite clusters (Fig. 5-2). Hardgrounds are formed where Surfaces of synsedimentarily cemented carbonate layers are exposed on the seafloor. Composite hardgrounds in mixed carbonate-siliciclastic successions typically cap packstone-grainstone beds with sharp base and overlying marl to

shale (Mclaughlin et al., 2008). Pyrite was formed by the early diagenetic replacement, and it indicates stratigraphic condensation. Thus, the upward carbonate increasing cycles is not shallowing upward but deepening upward with sediment starvation.

FA2 mainly consists of black shale (Bs), laminated lime-shale couplet (Lls). Lls which is tens of centimeters in thickness alternates with Bs. This facies association particularly appears at the middle part of the Machari Formation. FA2 was deposited in the calm condition with low carbonate production (Fig. 5-3). FA3 is composed of lime nodule-bearing shale (Sn) and anastomosed wackestone to packstone (Wpa). FA3 also shows cyclic successions but contains more carbonate content than FA1. In the depositional environment of FA3, carbonate production was increased by siliciclastic sediment starvation.

Table 5-1. Sedimentary facies of the Machari Formation

Lithofacies	**Description**	**Interpretation**
Black shale (Bs)	Black, laterally continuous lamination and fissility are developed (Fig. 5-1A).	Deposited by suspension settling (Elrick et al., 1991).
Laminated lime-shale couplet (Lls)	The color of this facies is light gray to gray. The part of the gray micrite laminae alternates with dark gray thin argillaceous laminae. This lamination is a few mm scale and well-stratified. Abrupt contact is observed with black shale facies (Fig. 5-1B).	Deposited from alternating suspension settling of carbonate and siliciclastic mud in the low-energy condition, and occasionally gravity flow by storm activity, (Markello and Read, 1981; Kim et al., 2014)
Bedded lime-shale couplet (Bls)	The color of this facies is gray to light gray. Good horizontal continuity and parallel layer are well developed in both the mudstone and carbonate parts. The carbonate part of the facies is a few mm to 5 cm and alternate with argillaceous lamination (Fig. 5-1C).	Deposited by turbidity current where siliciclastic mud settles almost in constant rate (Choi and Ryu, 2014)

Lime nodule-bearing shale (Sn)	Calcareous nodules show various shape such as oval and elongated shape. The thickness of nodule ranges from 1 to 15 cm, and nodules lie parallel to bedding plane. Lime nodule consists of micrite or wackestone, and surrounding by calcareous of dolomitic shale (Fig.5-1D).	Deposited from suspension fall out under low-energy condition and, low-density turbidity current within early diagenesis (Wanless, 1979)
Anastomosed wackestone to packstone (Wpa)	Light gray to gray massive or nodule shape limestone. It consists of lime mud and fossil fragments. Terrigenous silt to clay sized mud are distributed of irregular anastomosed shape (Fig.5-1E)	Deposited from subtidal and modification by compaction (Kwon et al., 2006)
Massive grainstone (Gm)	This facies shows light gray to gray color and generally consists of bioclasts, intra lasts, and pyrite, calcite sandstone. Calcite sandstone is composed of sand-sized limestone grains with micrite matrix and sparite. It erosionally contacts with underlying facies. Authigenic pyrite crust is condensed feature. (Fig. 5-1F)	High-energy, inner-ramp shoal and mid-ramp packstone; Deposited by wave agitation, or frequent storm reworking above storm wave base (Carlucci et al., 2014)

Table 5-2. Facies associations of the Machari Formation

Facies association	**Lithofacies**
FA1	black shale (Bs), laminated lime-shale couplet (Lls), bedded lime-shale couplet (Bls), lime nodule-bearing shale (Sn), and massive grainstone (Gm)
FA2	black shale (Bs), laminated lime-shale couplet (Lls)
FA3	lime nodule-bearing shale (Sn) and anastomosed wackestone to packstone (Wpa)

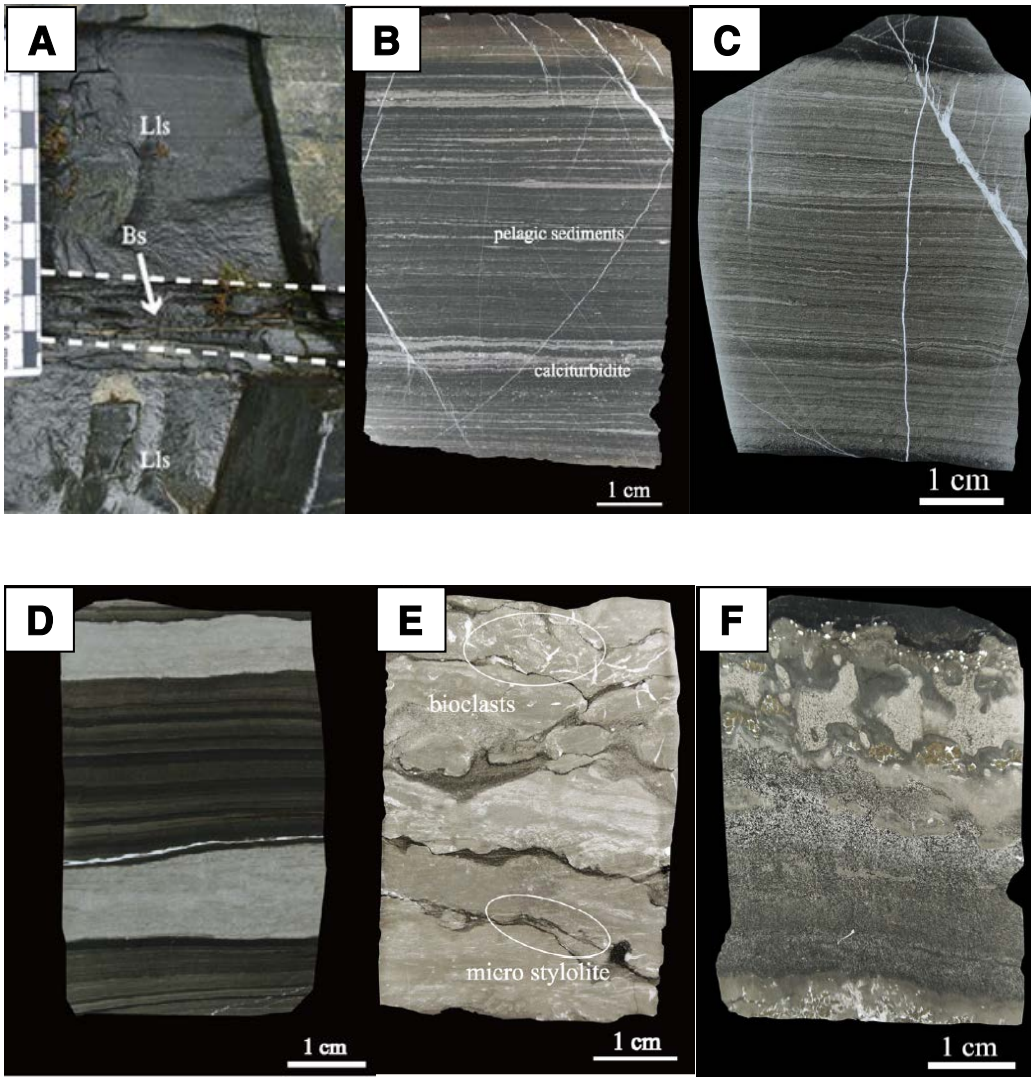

Fig. 5-1. Slab photographs showing lifhofacies of the Machari Formation at Deogwoo section. All slab photographs were quoted from Choi and Ryu (2014). (A) Black shale (Bs), (B) Laminated lime-shale couplet (Lls), (C) Bedded lime-shale couplet (Bls), (D) Lime nodule-bearing shale (Sn), (E) Anastomosed wackestone to packstone (Wpa), (F) Massive grainstone (Gm)

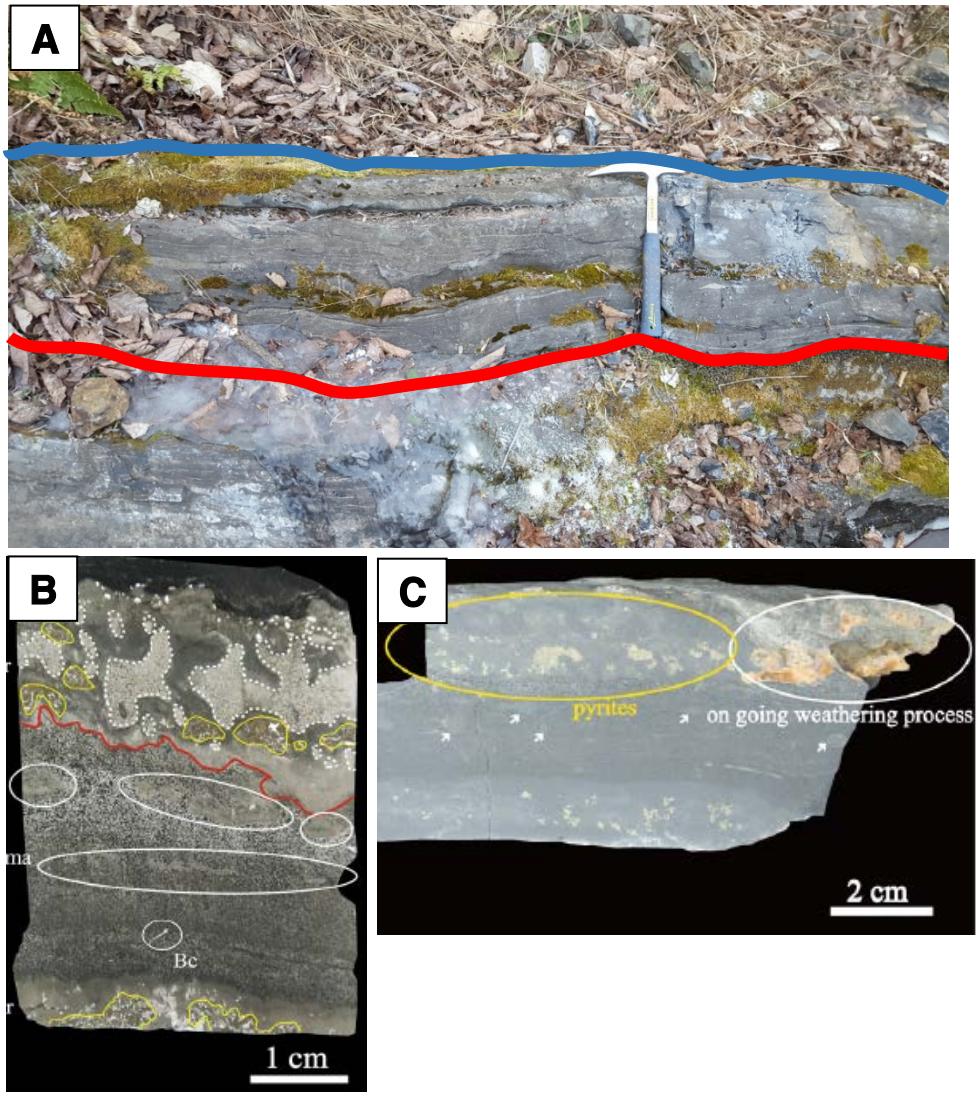

Fig. 5-2. Massive grainstone facies (A) Photograph of outcrop (hammer for scale is 26 cm long). (B), (C) Photograph of slab from Choi and Ryu (2014). Red line: erosional base, Yellow circle: pyrite clusters. White dotted line intraclasts which consisits of sand-sized calcite grains.

Fig. 5-3. Columnar section of the Machari formations at the Deogwoo section showing biostratigraphy, sequence stratigraphy, and variation of redeox-induced trace elements. In columnar section, Red line: sequence boundary, Dotted black line: maximum flooding surface, Green line: trilobite biozone boundary. In redox element plot, Red line: average shale values. Data plot of redox-induced elements is divided three sections: the lower, the middle, and the upper sections.

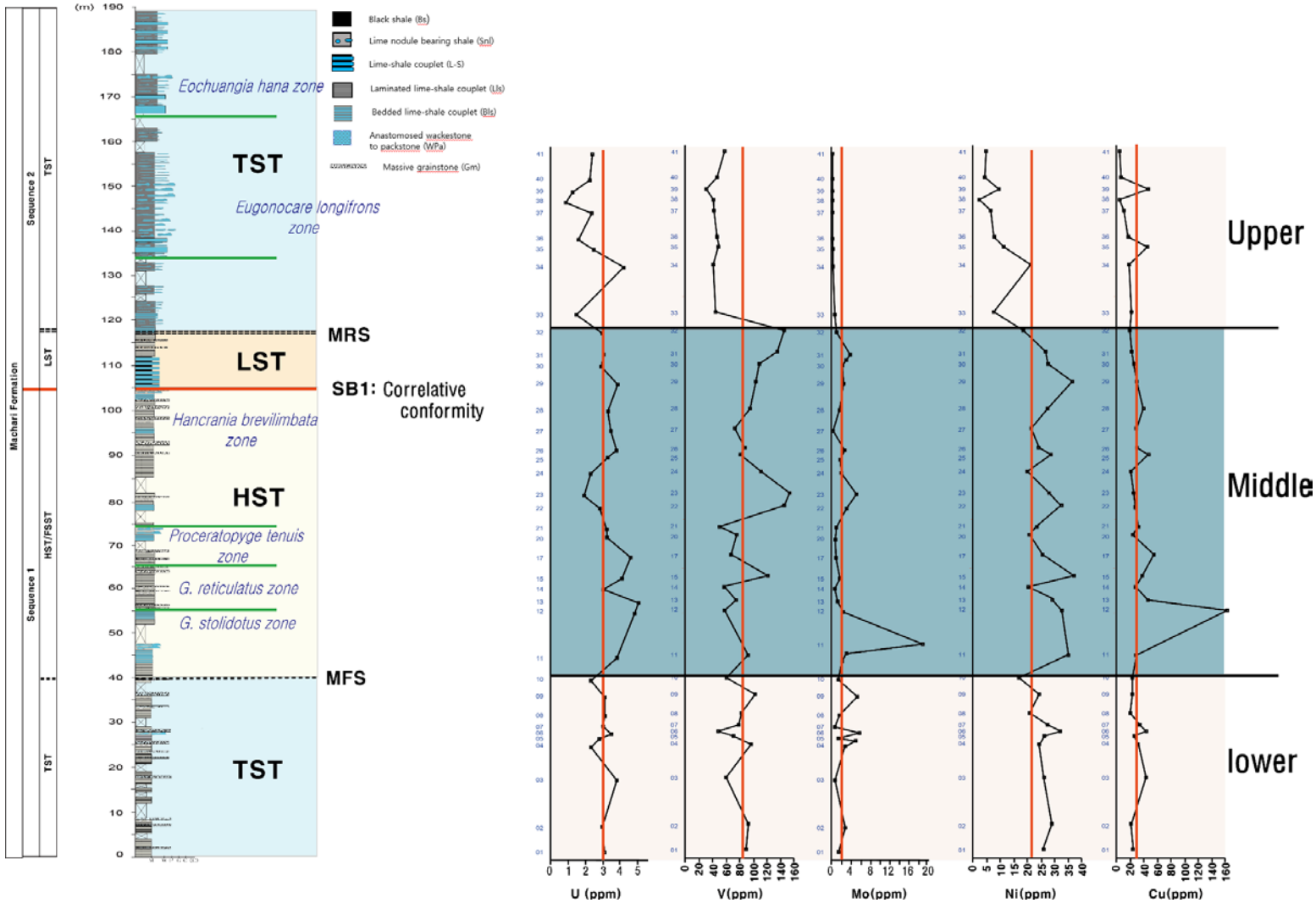
Machari Formation
Sequence 2
Sequence 1
TST
LST
HST/FSST
TST
(m)
Black shale (Bs)
Lime nodule bearing shale (Snl)
Lime-shale couplet (L-S)
Laminated lime-shale couplet (Lls)
Bedded lime-shale couplet (Bls)
Anastomosed wackestone to packstone (WPa)
Massive grainstone (Gm)
Eochuangia hana zone
TST
Eugonocare longifrons zone
MRS
LST
SB1: Correlative conformity
Hancrania brevilimbata zone
HST
Proceratopyge tenuis zone
G. reticulatus zone
G. stolidotus zone
MFS
TST
Upper
Middle
lower
U (ppm)
V(ppm)
Mo(ppm)
Ni(ppm)
Cu(ppm)

5.2. Sequence stratigraphy

The depositional setting of the Machari Formation was known as the continental slope (Chung and Lee, 1992) or carbonate ramp (Chung and Lee, 2002). During sea-level fall the Machari Formation does not seem to be exposed to subaerial condition since no karst features associated with sea-level fall has been found; therefore no unconformity is founded during sea-level lowstand (Chung et al., 2011). Machari Formation shows cyclic succession and consists of two sequences (Fig. 5-3).

In FA1, cycles which are composed of Bs, Lls, Bls, Sn, and Gm in ascending order representing the upward increase of carbonate. In this cycle, absences of components of full cycle exists due to relative controls of carbonate input, siliciclastic input, relative sea-level change, and degree of reworking. Thickness of Cycles at Lower part of Machari Formation ranges from 1 m to 3 m. This part represents TST characterized by relative thin cyclic succession. During base-level rise, condensed massive grainstone was frequently deposited by sediment starvation. TST is terminated by HST with the transition from 1-3 m scale cycles to 2-8 m scale cycles (Fig. 5-4). FA1 of HST contains more siliciclastic sediments compared to FA1 of TST. Lls of TST is characterized by distinct light gray calcareous lamination with black argillaceous lamination. However, Lls of HST is dominated by relatively siliciclastic lamination which indicates that siliciclastic sediment input from hinterland increased, thus, cycles of HST is thicker than that of TST. In the early HST, terrigenous sediments were rich resulted in raid deposition of mud layers. As the rate of progradation increased, the influx of detrital carbonate also increase and the

proportion of carbonate were increased in the late HST. FSST of mixed carbonate-siliciclastic settings probably shows a high-energy rippled calcislilitite and fine-grained grainstone which represents a time of rapid sea-level fall and progradation of laminated tidal and shoreface facies, not dependent on sediment supply (Carlucci et al., 2014). FSST is hardly divided from HST because of the absence of distinct evidence. HST abruptly terminated by LST which is composed of alternating Bs and Lls. The initial stage of base-level rise, sedimentation rate generally exceed the rate of accommodation created. Siliciclastic input prevented the formation of condensed bed and derived abundant shale facies. The absence of sandstone facies in the Machari Formation indicates the relative deeper setting.

SB1 of Machari Formation is also correlative conformity which has no distinct evidence of subaerial exposure such as desiccation cracks, fenestrae cavities, root casts, evaporate pseudomorphs, microbial laminites, paleosols, and paleokarst. Also, carbon isotope data from Chung et al. (2011) indicates that SB1 well matches with the peak of SPICE. FA1 changes to FA3 at the maximum regressive surface (MRS). FA3 is dominantly composed of carbonate facies (Sn and Wpa). TST of sequence 2 is located at the upper part of the Machari Formation. The upper part of the Machari Formation of deogwoo section represents TST which gradually increases Wpa facies, it means carbonate production increased by the decline of siliciclastic input.

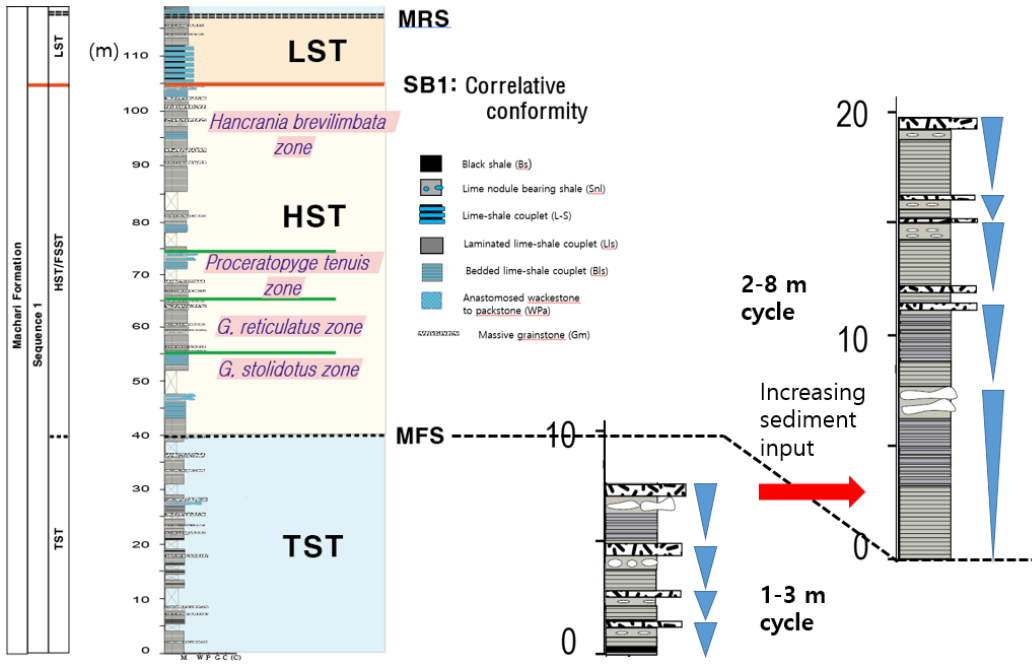

Fig. 5-4. Transition from 1-3 m scale cycles to 2-8 m scale cycles at MFS in Sequence 1

5.3. Redox condition

Several trace elements indicate the paleo-redox condition. Elements that bond to organic matter of make sulfide compounds enriched in strata under anoxic and euxinic conditions (Tribovillard et al., 2006; Straeten et al., 2011). Uranium (U), Vanadium (V), Molybdenum (Mo), Nickel (Ni), and Copper (Cu) are sensitive trace elements to redox and paleoproductivity conditions. They enrich in anoxic and euxinic conditions. Trace elements indicating the paleo-redox condition of Machari Formation are shown in Table 5-3. Excluding Mo, contents of U, V, Ni, Cu is less than that of average shale (Wedepohl,

1971, 1991). These deficient contents are due to lack of contents of trace elements in upper part of the Machari Formation. The trend of trace elements largely divides into three part; the lower (from DMC-1 to DMC-10), the middle (from DMC-11 to DMC-32), and the upper part (from DMC-33 to DM-33) (Fig. 5-3). In the lower part of Machari Formation, U, V, Mo, Ni, and Cu show relative flat trend and similar contents with average shale. Contents of U, V, Mo, and Ni start variable and enriched comparing with average shale excepting Cu in the middle part. Subsequently, U, V, Mo, Ni, Cu, abruptly drop compared to average shale in the upper part. These trend of variation in redox-induced trace elements is consistent with sequence stratigraphic analysis. The lower part coincides with TST of sequence 1, and the middle part consistent with HST and FSST of sequence 1 and LST of sequence 2.

The upper part of the Machari Formation concordant with TST of sequence 2. Myrow et al. (2012) suggested deepening upward cycle, and it accounts for trend of redox-induced elements in Machari Formation. When the regressive phase, input of siliciclastic mud results in suppression of carbonate production, and oxygen stratification is subsequently generated by a brackish-water surface layer that makes stabilization of water column and reduces vertical circulation which leads to benthic oxygen depletion (Myrow et al., 2012). Thus, starting with regressive HST of sequence 1, redox-induced elements enriched in strata of Machari Formation after MFS. Highly variation of redox-induced elements in HST of sequence 1 is caused by higher-order cycles. FSST and LST in the middle part show enriched U, V, Mo, and Ni. In the TST of sequence 1, redox-induced elements rapidly

decrease by breakdown in water stratification with enhanced circulation which led to fully oxygenated benthic condition and promoted biogenic carbonate production.

Table 5-3. Contents and mean values (ppm) of selected trace elements in the Machari Formation.

Sample	U	V	Mo	Ni	Cu (ppm)
DMC-1	3.1	110.9	1.7	26.4	23.1
DMC-2	2.9	95.8	2.7	29.6	19.8
DMC-3	3.7	85.8	1.0	26.5	40.9
DMC-4	2.4	80.9	2.5	24.9	31.4
DMC-5	2.8	80.0	1.5	27.0	24.5
DMC-6	3.4	66.9	7.3	32.5	40.0
DMC-7	3.0	118.4	1.1	28.0	32.0
DMC-8	3.1	95.2	1.7	21.3	18.7
DMC-9	3.0	106.8	5.0	24.8	21.3
DMC-10	2.3	66.8	1.5	17.1	21.5
DMC-11	3.9	100.6	18.5	35.8	26.7
DMC-12	4.8	83.8	3.6	32.9	161.7
DMC-13	5.0	89.1	1.4	29.4	42.8
DMC-14	3.0	69.2	0.8	20.5	27.3
DMC-15	4.0	159.9	2.3	37.9	35.6
DMC-17	4.6	87.2	1.2	26.0	53.6
DMC-20	3.2	73.6	0.8	21.2	21.9
DMC-21	3.2	59.6	1.1	23.9	30.3
DMC-22	2.8	128.7	2.5	33.3	25.4
DMC-23	1.9	162.8	4.9	28.4	24.8
DMC-24	2.3	101.8	1.9	20.3	19.5
DMC-25	3.3	108.9	2.2	29.1	45.6

(Continued)

DMC-26	3.8	87.9	2.4	24.3	28.8
DMC-27	3.5	103.7	0.3	21.6	28.7
DMC-28	3.3	109.8	1.7	27.9	38.6
DMC-29	3.8	121.0	2.7	37.3	28.2
DMC-30	2.9	108.5	2.0	28.1	25.4
DMC-31	3.0	153.5	4.0	27.0	21.3
DMC-32	3.0	115.8	0.7	18.7	18.7
DMC-33	1.4	26.8	0.4	7.9	21.3
DMC-34	4.2	50.2	0.5	21.5	17.6
DMC-35	2.4	34.3	0.2	11.5	43.2
DMC-36	1.5	35.0	0.1	7.7	15.6
DMC-37	2.2	35.0	0.2	6.5	8.3
DMC-38	0.9	21.6	0.1	2.5	2.8
DMC-39	1.2	29.8	0.1	9.3	45.6
DMC-40	2.2	54.1	0.1	4.3	6.2
DMC-41	2.4	62.4	0.1	4.6	3.8
DM-30	3.8	54.1	0.1	11.0	2.0
DM-32	1.6	56.7	0.3	23.0	34.6
DM-33	5.4	37.7	0.1	9.3	11.6
average	3.0	83.7	2.0	22.0	29.0
AS	3.7	130.0	1.3	68.0	45.0

AS: average shale values from Wedepohl (1971, 1991)

6. Interregional comparison

The Taebaeksan basin located at the eastern margin of the North China platform during the early Paleozoic (Chough et al., 2000; Kwon et al., 2006). Yeongweol unit of Taebeksan basin was also included in SKB, which is suggested by the trilobite assemblages. However, the paleogeographic position of the Yeongweol platform has been considerably debated (Cluzel et al., 1991; Yin and Nie, 1993; Kwon, 2012). Recently, based on detrital zircon geochronology and Nd isotopic data, the southern margin of the SKB was adjacent to the northern margin of East Gondwana (McKenzie et al., 2013; Lee et al., 2016). Although specific position is enigmatic, North China platform and Taebaek and Yeongweol units of Taebaeksan basin were probably sourced detritus from East Gondwana, and they were located in mixed carbonate-siliciclastic environment which is influenced both by siliciclastic input and in-situ carbonate production (Fig. 6-1). North China platform and Taebaek and Yeongweol units of Taebaeksan basin was an extensive epeiric platform and tectonically stable during the Cambrian (Lee and Lee, 2003; Kwon et al., 2006). Thus, sequence stratigraphic framework of North China platform and Taebaeksan basin has to be done with consideration about siliciclastic input from Eastern Gondwana, not only from regional terrigenous input. Previous studies of sequence stratigraphic analysis have conducted not with consideration of outside sediments. Interregional comparison between Taebaek and Yeongweol units of Taebaeksan basin and North China platform is performed by biostratigraphic and sequence stratigraphic data (Fig. 6-2).

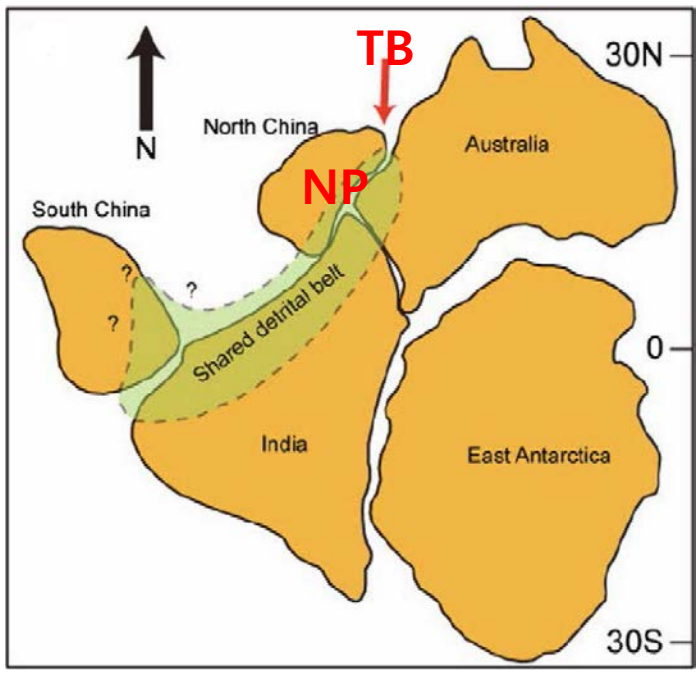

Fig. 6-1. Paleogeographic reconstrutions of East Gondwana during the latest Cambrian (MaKenzie et al., 2011; Lee et al., 2016). Red arrow indicates the location of the Korean Peninsula in the SKB.

Fig. 6-2. Interregional correlation with Taebaek and Yeongweol units of Taebaeksan basin and North China platform with biostratigraphic and sequence stratigraphic data. Taebaek: The Sesong and Hwajeol formations, Yeongweol: The Machari Formation, Shandong: The Gushan and Chaomidian formations. Relative sea-level curve was modified from Chen et al. (2014).

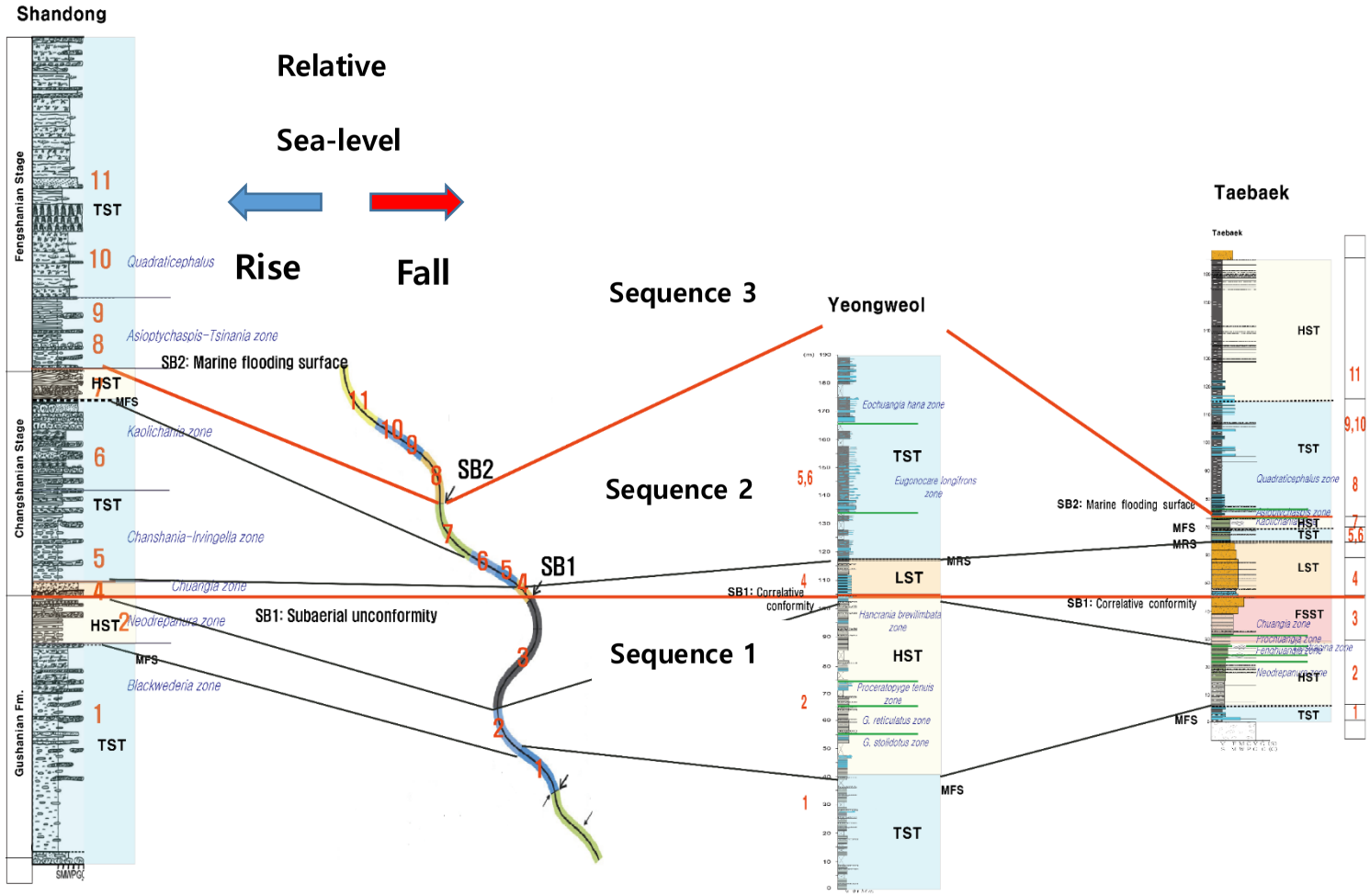
Shandong
Relative
Sea-level
Rise
Fall
Fengshanian Stage
Changshanian Stage
Gushanian Fm.
11
TST
10
Quadraticephalus
9
8
Asioptychaspis-Tsinania zone
SB2: Marine flooding surface
HST
MFS
Kaolichania zone
6
TST
Chanshania-Irvingella zone
5
4
Chuangia zone
HST
2
Neodrepanura zone
SB1: Subaerial unconformity
MFS
Blackwederia zone
1
TST
Sequence 3
Sequence 2
Sequence 1
SB2
SB1
Yeongweol
Eochuangia hana zone
TST
Euganocare longifrons zone
5,6
SB2: Marine flooding surface
MFS
MRS
LST
SB1: Correlative conformity
4
Hancrania brevilimbata zone
HST
Proceratopyge tenuis zone
G. reticulatus zone
G. stolidotus zone
2
MFS
1
TST
Taebaek
HST
11
TST
9,10
Quadraticephalus zone
8
HST
7
TST
5,6
LST
4
FSST
3
Chuangia zone
Prochuangia zone
Fengchengia zone
Neodrepanura zone
HST
2
TST
1
MFS

Late Cambrian Shandong, Yeongweol, and Taebaek successions are correlated with sequence stratigraphic surface (Fig. 6-2). In sequence 1, maximum flooding surface (MFS) formed above *Blackwederia* zone in Shangdong, below *G. stolidotus* zone in Yeongweol, and below *Neodrepanura* zone in Taebaek. MFS well coincides with biozone correlation. SB1 in Shandong region shows extensive subaerial unconformity with missing *Prochuangia* zone. SB1 in Taebaeksan basin represents as a correlative conformity. SB1 is discovered at *Hancrania brenilmbata* zone in Yeongweol and above *Chuangia* zone in Taebaek. In the Shandong region, subaerial erosion and non-deposition were occurred during rapid sea-level fall, whereas succession of FSST was deposited at Taebaek region.

In sequence 2, LST deposits represent thin grainstone, and TST deposits show relative thick succession in Shangdong region. While Taebaek region displays thick progradational to aggradational succession of LST and thin condensed TST deposits. In Yeongweol region, moderately thick LST was deposited as alternating shale and laminated limestone which indicates that Yeongweol area was influenced by both terrigenous input and carbonate input (Fig. 6-2). Thus, this alternating lime-shale implies that siliciclastic input and carbonate production was occurred alternatively by higher-order sea-level changes. In TST, as terrigenous sediments were starved, carbonate production were increased. As a result, carbonate platform of Shandong region starts to catch-up and keep-up. Lee et al. (2012) postulate sequence boundary at transition boundary between flat-bedded microbialite and domal microbialite which could occur when relative sea-level rise. They set sequence boundary based on the change of trajectory from carbonate progradation to retrogradation

and named flooding surface. However, there was no decline of the rate of base-level rise in coeval strata of Sesong Formation at Taebaek region. Furthermore, the boundary between Changshanian stage and Fengshanian stage represents an abrupt facies change from grainstone with HSC to shale. We reinterpreted that this boundary is sequence boundary between sequence 2 and sequence 3 and also laid between *Kaolishania* zone and *Asiptychaspi*s zone both of Shandong and Taebaek regions. SB2 of Taebaek region shows abrupt changes from fine-grained sandstone to lime-shale couplet which were changed by abrupt base-level rise, and this boundary must be flooding surface.

In sequence 3, carbonate production was increased by abrupt base-level rise and entirely siliciclastic sediments was starved. Thus, carbonate platform interior was developed at Shandong region and carbonate-dominant facies such as anastomosed wacke to packstone and lime nodule-bearing shale with no coarse siliciclastic deposits at Taebaeksan basin.

Sedimentary basins in North China and the Korean Peninsula were located in a stable equatorial to subequatorial craton during Cambrian (Meng et al., 1997; Lee and Lee., 2003), which suggests that slow thermal subsidence was the basin-forming mechanism. With absence of tectonic activity, the timing of sequence and generation of bounding surface were dominantly developed by eustasy (Sim and Lee, 2006). Thus, controls of tectonics in the relative sea-level changes could be limited in both basins. With the relative sea-level fall, siliciclastic input was increased by basinward shoreline migration, and carbonate production was declined. Therefore thick siliciclastic sediments were deposited in siliciclastic margin (Taebaek region), and marl to shale dominant succession with hiatus

were deposited in carbonate platform (Shandong region). As relative sea-level rise, siliciclastic sediments input was reduced by landward shoreline migration and river alluviation, and carbonate productivity was increased. In the carbonate platform, carbonate production was increased, whereas condensed section was developed in siliciclastic margin (Fig. 6-3).

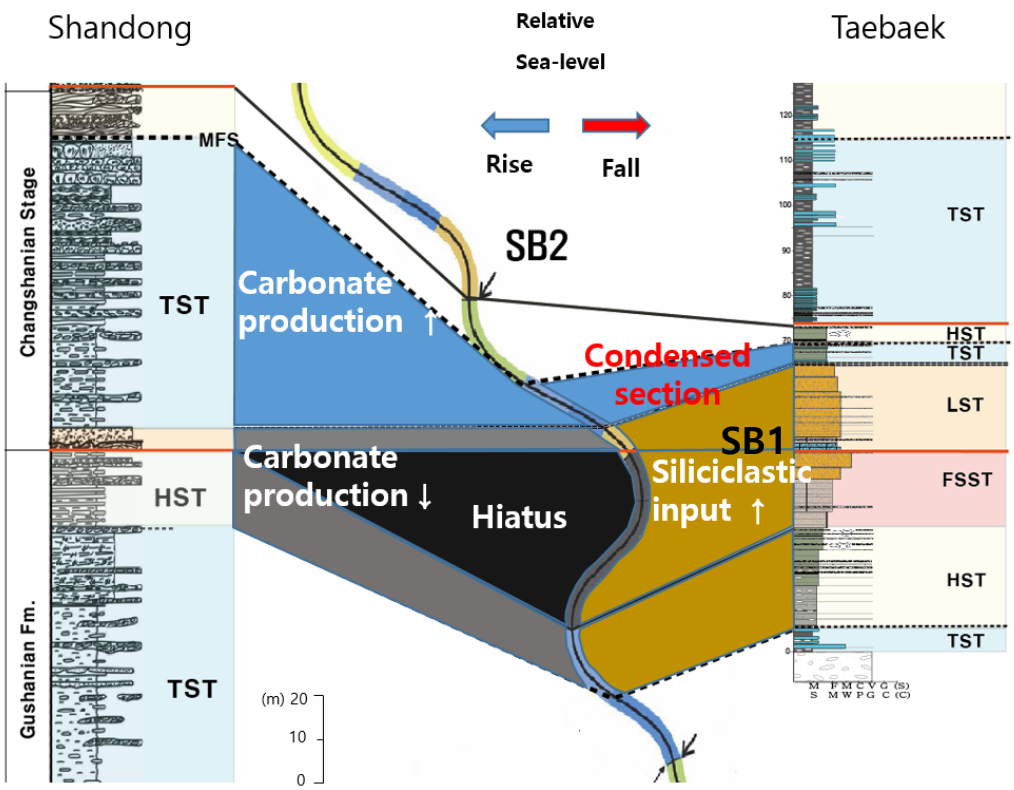

Fig. 6-3. Interplay between siliciclastic input and carbonate production rate based on relative sea-level fluctuation

7. Conclusion

The upper Cambrian Series 3 to Furongian Sesong and Hwajeol formations in Taebeak area consist mainly of siliciclastic sediment with alternating carbonate, and Machari Formation in Yeongweol area is comprised of alternating shale and carbonate which was deposited in deeper settings, which were formed in the mixed carbonate-siliciclasitc stable epeiric sea environment. Sequence stratigraphic analysis reveals that the Sesong and Hwajeol formations are composed of three stratigraphic sequences with two bounding surfaces, and the Machari Formation consists of two stratigraphic sequences with a sequence boundary. Chemostratigraphy conducted by using the stable carbon isotope in Sesong and Hwajeol formations and redox-induced trace elements supports sequence stratigraphic interpretation. Late Cambrian Gushan and Chamodidian formations in Shandong region which are coeval strata of Taebaeksan basin were correlated based on sequence stratigraphic interpretation and trilobite biozone. Siliciclastic input and carbonate productivity interplay each other in the mixed carbonate-siliciclastic environment. Previous workers have not been considered the terrigenous source from outside which recently regards as deriving from East Gondwana. Transition into shaley facies of carbonate platform is simply not responsible for the base-level rise. When considering the sequence stratigraphy in the mixed carbonate-siliciclastic epeiric platform, we have to deliberate complexity of interplay siliciclastic input and carbonate production compared to pure carbonate platforms and siliciclastic margins.

References

Ahlberg, P., et al. (2009). "Cambrian high-resolution biostratigraphy and carbon isotope chemostratigraphy in Scania, Sweden: first record of the SPICE and DICE excursions in Scandinavia." Lethaia **42**(1): 2-16.

Blair, T. C. and J. G. McPherson (1999). "Grain-size and textural classification of coarse sedimentary particles." Journal of Sedimentary Research **69**(1).

Buggisch, W., et al. (2003). "Carbon isotope record of Late Cambrian to Early Ordovician carbonates of the Argentine Precordillera." Palaeogeography, Palaeoclimatology, Palaeoecology **195**(3): 357-373.

Burchette, T. and V. Wright (1992). "Carbonate ramp depositional systems." Sedimentary Geology **79**(1-4): 3-57.

Carlucci, J. R., et al. (2014). "Facies architecture and sequence stratigraphy of the Ordovician Bromide Formation (Oklahoma): a new perspective on a mixed carbonate-siliciclastic ramp." Facies **60**(4): 987-1012.

Catuneanu, O. (2006). Principles of sequence stratigraphy, Elsevier.

Catuneanu, O., et al. (2011). "Sequence stratigraphy: methodology and nomenclature." Newsletters on stratigraphy **44**(3): 173-245.

Chen, J., et al. (2011). "An extensive erosion surface of a strongly deformed limestone bed in the Gushan and Chaomidian formations (late Middle Cambrian to Furongian), Shandong Province, China: Sequence–stratigraphic implications." Sedimentary Geology **233**(1): 129-149.

Chen, J., et al. (2012). "Sequence-stratigraphic comparison of the upper Cambrian Series 3 to Furongian succession between the Shandong region, China and the Taebaek area, Korea: high variability of bounding surfaces in an epeiric platform." Geosciences Journal **16**(4): 357-379.

Chen, J., et al. (2009). "Limestone pseudoconglomerates in the Late Cambrian Gushan and

Chaomidian Formations (Shandong Province, China): soft-sediment deformation induced by storm-wave loading." Sedimentology **56**(4): 1174-1195.

Chen, J. and H. S. Lee (2013). "Soft-sediment deformation structures in Cambrian siliciclastic and carbonate storm deposits (Shandong Province, China): Differential liquefaction and fluidization triggered by storm-wave loading." Sedimentary Geology **288**: 81-94.

Chen, J., et al. (2014). "Formative mechanisms, depositional processes, and geological implications of Furongian (late Cambrian) reefs in the North China Platform." Palaeogeography, Palaeoclimatology, Palaeoecology **414**: 246-259.

Choi and Ryu (2013). "Carbonate sequence stratigraphy of the Cambrian Machari Formation, Taebaeksan Basin" Unpublished Ms. D. dissertration, Kyungpook National University

Choi, D., et al. (2001). "Ordovician trilobite faunas and depositional history of the Taebaeksan Basin, Korea: implications for palaeogeography." Alcheringa **25**(1): 53-68.

Choi, D. K. (1998). "The Yongwol Group (Cambrian-Ordovician) redefined: a proposal for the stratigraphic nomenclature of the Choson Supergroup." Geosciences Journal **2**(4): 220-234.

Choi, D. K. (2007). "Trilobite research in South Korea during the 20th Century." Bulletin of the New York State Museum **407**: 81-96.

Choi, D. K., et al. (2004). "Taebaek group (Cambrian-Ordovician) in the Seokgaejae section, Taebaeksan Basin: a refined lower Paleozoic stratigraphy in Korea." Geosciences Journal **8**(2): 125-151.

Choi, D. K. and E. Y. Kim (2006). "Occurrence of Changshania (Trilobita, Cambrian) in the Taebaeksan Basin, Korea and its stratigraphic and paleogeographic significance." Palaeogeography, Palaeoclimatology, Palaeoecology **242**(3): 343-354.

Choi, D. K., et al. (2004). "Upper Cambrian agnostoid trilobites from the Machari

formation, Yongwol, Korea." Geobios **37**(2): 159-189.

Chough, S., et al. (2000). "Tectonic and sedimentary evolution of the Korean peninsula: a review and new view." Earth-Science Reviews **52**(1): 175-235.

Chough, S. K., et al. (2010). "Cambrian stratigraphy of the North China Platform: revisiting principal sections in Shandong Province, China." Geosciences Journal **14**(3): 235.

Chung, G.-S. and E.-K. Lee (2002). "Depositional Environment of the Cambrian Machari Formation in the Yeongweol Area, Gangweon Province, Korea." Journal of the Korean earth science society **23**(1): 72-86.

Chung, G.-S., et al. (2011). "Stable Carbon Isotope Stratigraphy of the Cambrian Machari Formation in the Yeongweol Area, Gangweon Province, Korea." Journal of the Korean earth science society **32**(5): 437-452.

Chung, G. S. and L. S. Land (1997). "Dolomitization of the periplatform carbonate slope deposit, the Machari Formation (Middle to Late Cambrian), Korea." Carbonates and Evaporites **12**(2): 163-176.

Chung, K. and E. Lee (1992). "Diagenesis of the Machari Formation (Upper Cambrian) in the Yeongweol Area, Kangweon-do, Korea." Sedimentary basins in the Korean Peninsula and adjacent seas. Hallimwon Publishing Co., Seoul, Korea **104128**.

Cluzel, D., et al. (1991). "Early Middle Paleozoic intraplate orogeny in the Ogcheon belt (South Korea): a new insight on the Paleozoic buildup of East Asia." Tectonics **10**(6): 1130-1151.

D'agostini, D. P., et al. (2015). "The Modern Mixed Carbonate–Siliciclastic Abrolhos Shelf: Implications For A Mixed Depositional Model." Journal of Sedimentary Research **85**(2): 124-139.

Dahl, T. W., et al. (2014). "Uranium isotopes distinguish two geochemically distinct stages during the later Cambrian SPICE event." Earth and planetary science letters **401**: 313-326.

Elrick, M., et al. (1991). "Short-term paleoclimatic fluctuations expressed in lower Mississippian ramp-slope deposits, southwestern Montana." Geology **19**(8): 799-802.

Elrick, M., et al. (2011). "Oxygen-isotope trends and seawater temperature changes across the Late Cambrian Steptoean positive carbon-isotope excursion (SPICE event)." Geology **39**(10): 987-990.

Elrick, M. and A. C. Snider (2002). "Deep-water stratigraphic cyclicity and carbonate mud mound development in the Middle Cambrian Marjum Formation, House Range, Utah, USA." Sedimentology **49**(5): 1021-1047.

Eoff, J. D. (2014a). "Sequence stratigraphy of the Upper Cambrian (Furongian; Jiangshanian and Sunwaptan) Tunnel City Group, Upper Mississippi Valley: transgressing assumptions of cratonic flooding." Sedimentary Geology **302**: 87-101.

Eoff, J. D. (2014b). "Sedimentary facies of the upper Cambrian (Furongian; Jiangshanian and Sunwaptan) Tunnel City Group, Upper Mississippi Valley: new insight on the old stormy debate." Sedimentary Geology **302**: 102-121.

Ergaliev, G. K. (1980). "Trilobites of the Middle and Upper Cambrian of the Maly Karatau." Akademiya Nauk Kazakhskoy SSR, Institut Geologicheskikh Nauk **20**.

Föllmi, K. B. (2016). "Sedimentary condensation." Earth-Science Reviews **152**: 143-180.

Gill, B. C., et al. (2011). "Geochemical evidence for widespread euxinia in the Later Cambrian ocean." Nature **469**(7328): 80-83.

Gillespie, J. L. and C. S. Nelson (1996). "Distribution and control of mixed terrigenous-carbonate surficial sediment facies, Wanganui shelf, New Zealand." New Zealand Journal of Geology and Geophysics **39**(4): 533-549.

Glumac, B. and M. L. Spivak-Birndorf (2002). "Stable isotopes of carbon as an invaluable stratigraphic tool: An example from the Cambrian of the northern Appalachians, USA." Geology **30**(6): 563-566.

Glumac, B. and K. R. Walker (2000). "Carbonate deposition and sequence stratigraphy of

the terminal Cambrian grand cycle in the southern Appalachians, USA." Journal of Sedimentary Research **70**(4): 952-963.

Hong, P. S., et al. (2003). "Trilobites from the Lejopyge armata Zone (upper Middle Cambrian) of the Machari Formation, Yongwol Group, Korea." Journal of Paleontology **77**(05): 895-907.

Hwang, H.-A. and D. K. Choi (2005). "Heterochrony of the Late Cambrian olenid trilobites from the Machari Formation, Yeongwol, Korea: implications for biostratigraphy and intercontinental correlation." Geosciences Journal **9**(2): 215-222.

Jongsun, H., et al. (2016). "Distribution of Chancelloriids in a Middle Cambrian Carbonate Platform Deposit, Taebaek Group, Korea." Acta Geologica Sinica (English Edition) **90**(3): 783-795.

Kim, J. C. and Y. I. Lee (1998). "Cyclostratigraphy of the Lower Ordovician Dumugol Formation, Korea: meter-scale cyclicity and sequence-stratigraphic interpretation." Geosciences Journal **2**(3): 134-147.

Kim, Y.-H. G., et al. (2014). "Depositional systems of the Lower Ordovician Mungok Formation in Yeongwol, Korea: implications for the carbonate ramp facies development." Geosciences Journal **18**(4): 397-417.

Kim, Y. and Y. I. Lee (2004). "Diagenesis of shallow marine sandstones, the Lower Ordovician Dongjeom Formation, Korea: response to relative sea-level changes." Journal of Asian Earth Sciences **23**(2): 235-245.

Kouchinsky, A., et al. (2008). "The SPICE carbon isotope excursion in Siberia: a combined study of the upper Middle Cambrian–lowermost Ordovician Kulyumbe River section, northwestern Siberian Platform." Geological Magazine **145**(05): 609-622.

Kump, L., et al. (1999). "A weathering hypothesis for glaciation at high atmospheric pCO 2 during the Late Ordovician." Palaeogeography, Palaeoclimatology, Palaeoecology **152**(1): 173-187.

Kump, L. R. (1991). "Interpreting carbon-isotope excursions: Strangelove oceans." Geology **19**(4): 299-302.

Kump, L. R. (2008). "The rise of atmospheric oxygen." Nature **451**(7176): 277-278.

Kwon, Y. (2012). "Sequence Stratigraphy of the Yeongweol Group (Cambrian-Ordovician), Taebaeksan Basin, Korea: Paleogeographic Implications." Economic and Environmental Geology **45**(3): 317-333.

Kwon, Y., et al. (2002). "Origin of limestone conglomerates in the Choson Supergroup (Cambro–Ordovician), mid-east Korea." Sedimentary Geology **146**(3): 265-283.

Kwon, Y., et al. (2006). "Sequence stratigraphy of the Taebaek Group (Cambrian–Ordovician), mideast Korea." Sedimentary Geology **192**(1): 19-55.

Kwon, Y. K. and S. K. Chough (2005). "Sequence stratigraphy of the cyclic successions in the Dumugol Formation (Lower Ordovician), mideast Korea." Geosciences Journal **9**(4): 305-324.

Łabaj, M. A. and B. R. Pratt (2016). "Depositional Dynamics In A Mixed Carbonate–Siliciclastic System: Middle–Upper Cambrian Abrigo Formation, Southeastern Arizona, USA." Journal of Sedimentary Research **86**(1): 11-37.

Lazar, O. R., et al. (2015). "Capturing key attributes of fine-grained sedimentary rocks in outcrops, cores, and thin sections: nomenclature and description guidelines." Journal of Sedimentary Research **85**(3): 230-246.

Lee, J.-H., et al. (2010). "Paleoenvironmental implications of an extensive maceriate microbialite bed in the Furongian Chaomidian Formation, Shandong Province, China." Palaeogeography, Palaeoclimatology, Palaeoecology **297**(3): 621-632.

Lee, J.-H., et al. (2012). "Demise of an extensive biostromal microbialite in the Furongian (late Cambrian) Chaomidian Formation, Shandong Province, China." Geosciences Journal **16**(3): 275-287.

Lee, J.-H., et al. (2015). "The middle–late Cambrian reef transition and related geological events: A review and new view." Earth-Science Reviews **145**: 66-84.

LEE, J. G. and D. K. CHOI (1994). "Glyptagnostus and associated trilobites from the

Machari Formation, Yeongweol, Korea." 고생물학회지 **10**(1): 117-136.

LEE, J. G. and D. K. CHOI (1995). "Late Cambrian trilobites from the Machari Formation, Yeongweol-Machari area, Korea." 고생물학회지 **11**(1): 1-46.

Lee, Y. I., et al. (2016). "Detrital zircon geochronology and Nd isotope geochemistry of the basal succession of the Taebaeksan Basin, South Korea: Implications for the Gondwana linkage of the Sino-Korean (North China) block during the Neoproterozoic–early Cambrian." Palaeogeography, Palaeoclimatology, Palaeoecology **441**: 770-786.

Lim, J. N., et al. (2015). "Lithofacies and Stable Carbon Isotope Stratigraphy of the Cambrian Sesong Formation in the Taebaeksan Basin, Korea." Journal of the Korean earth science society **36**(7): 617-631.

Loi, A. and M.-P. Dabard (2002). "Controls of sea level fluctuations on the formation of Ordovician siliceous nodules in terrigenous offshore environments." Sedimentary Geology **153**(3): 65-84.

Lu, Y. and H. Lin (1989). The Cambrian trilobites of western Zhejiang, Science press Beijing.

Markello, J. and J. Read (1981). "Carbonate ramp-to-deeper shale shelf transitions of an Upper Cambrian intrashelf basin, Nolichucky Formation, Southwest Virginia Appalachians." Sedimentology **28**(4): 573-597.

McKenzie, N. R., et al. (2011). "Trilobites and zircons link north China with the eastern Himalaya during the Cambrian." Geology **39**(6): 591-594.

McLaughlin, P. I., et al. (2008). "Hierarchy of sedimentary discontinuity surfaces and condensed beds from the middle Paleozoic of eastern North America: implications for cratonic sequence stratigraphy." Geological Association of Canada Special Paper **48**: 175-200.

Meng, X., et al. (1997). "Sequence Sequence stratigraphy, sea-level changes and depositional systems in the Cambro-Ordovician of the North China carbonate

platform." Sedimentary Geology **114**(1): 189-222.

Myrow, P. M., et al. (2012). "Mixed siliciclastic–carbonate upward-deepening cycles of the upper Cambrian inner detrital belt of Laurentia." Journal of Sedimentary Research **82**(4): 216-231.

Nemec, W. (1990). "Aspects of sediment movement on steep delta slopes." Coarse-grained deltas **10**: 29-73.

O'Brien, N. R. (1996). "Shale lamination and sedimentary processes." Geological Society, London, Special Publications **116**(1): 23-36.

Palmer, A. R. (1960). Trilobites of the Upper Cambrian Dunderberg Shale, Eureka District, Nevada, US Government Printing Office.

Park, T.-Y. and D. K. Choi (2011). "Trilobite faunal successions across the base of the Furongian Series in the Taebaek Group, Taebaeksan Basin, Korea." Geobios **44**(5): 481-498.

Park, T.-Y., et al. (2013). "Late middle Cambrian (Cambrian Series 3) trilobite faunas from the lowermost part of the Sesong Formation, Korea and their correlation with North China." Journal of Paleontology **87**(06): 991-1003.

Park, T.-Y., et al. (2012). "Middle Furongian (late Cambrian) polymerid trilobites from the upper part of the Sesong Formation, Taebaeksan Basin, Korea." Geosciences Journal **16**(4): 381-398.

PARK, T. Y. S., et al. (2016). "Cambrian Stem-group Cnidarians with a New Species from the Cambrian Series 3 of the Taebaeksan Basin, Korea." Acta Geologica Sinica (English Edition) **90**(3): 827-837.

Peters, S. E. and R. R. Gaines (2012). "Formation of the/Great Unconformity/'as a trigger for the Cambrian explosion." Nature **484**(7394): 363-366.

Runkel, A. C., et al. (1998). "Origin of a classic cratonic sheet sandstone: Stratigraphy across the Sauk II–Sauk III boundary in the Upper Mississippi Valley." Geological Society of America Bulletin **110**(2): 188-210.

Runkel, A. C., et al. (2007). "High-resolution sequence stratigraphy of lower Paleozoic sheet sandstones in central North America: The role of special conditions of cratonic interiors in development of stratal architecture." Geological Society of America Bulletin **119**(7-8): 860-881.

Ryu, I.-C., et al. (2005). "A middle Ordovician drowning unconformity on the northeastern flank of the Okcheon (Ogcheon) belt, south Korea." Gondwana Research **8**(4): 511-528.

Ryu, I.-C., et al. (2009). "Geochemical Study of the Jigunsan Shale: A Sequence Stratigraphic Application to Defining a Middle Ordovician Condensed Section, Taebacksan (Taebaeksan) Basin." Economic and Environmental Geology **42**(1): 27-53.

Saltzman, M. R. (2005). "Phosphorus, nitrogen, and the redox evolution of the Paleozoic oceans." Geology **33**(7): 573-576.

Saltzman, M. R., et al. (2004). "The Late Cambrian Spice (13C) Event and the Sauk II-SAUK III Regression: New Evidence from Laurentian Basins in Utah, Iowa, and Newfoundland." Journal of Sedimentary Research **74**(3): 366-377.

Saltzman, M. R., et al. (2015). "Persistent oceanic anoxia and elevated extinction rates separate the Cambrian and Ordovician radiations." Geology **43**(9): 807-810.

Saltzman, M. R., et al. (2000). "A global carbon isotope excursion (SPICE) during the Late Cambrian: relation to trilobite extinctions, organic-matter burial and sea level." Palaeogeography, Palaeoclimatology, Palaeoecology **162**(3): 211-223.

Saltzman, M. R., et al. (1998). "Carbon isotope stratigraphy of Upper Cambrian (Steptoean Stage) sequences of the eastern Great Basin: Record of a global oceanographic event." Geological Society of America Bulletin **110**(3): 285-297.

Saltzman, M. R., et al. (2011). "Pulse of atmospheric oxygen during the late Cambrian." Proceedings of the National Academy of Sciences **108**(10): 3876-3881.

Schlager, W. (1992). "Sedimentology and sequence stratigraphy of reefs and carbonate

platforms."

Schlager, W., et al. (1994). "Highstand shedding of carbonate platforms." Journal of Sedimentary Research **64**(3).

Sim, M. S. and Y. I. Lee (2006). "Sequence stratigraphy of the Middle Cambrian Daegi Formation (Korea), and its bearing on the regional stratigraphic correlation." Sedimentary Geology **191**(3): 151-169.

Sloss, L. (1963). "Sequences in the cratonic interior of North America." Geological Society of America Bulletin **74**(2): 93-114.

Smith, M. P. and D. A. Harper (2013). "Causes of the Cambrian explosion." Science **341**(6152): 1355-1356.

Sohn, J. W. and D. K. Choi (2007). "Furongian trilobites from theAsioptychaspis andQuadraticephalus zones of the Hwajeol Formation, Taebaeksan Basin, Korea." Geosciences Journal **11**(4): 297-314.

Tribovillard, N., et al. (2006). "Trace metals as paleoredox and paleoproductivity proxies: an update." Chemical geology **232**(1): 12-32.

Tucker, M. (1985). "Shallow-marine carbonate facies and facies models." Geological Society, London, Special Publications **18**(1): 147-169.

Tucker, M. E. (2003). "Mixed clastic–carbonate cycles and sequences: Quaternary of Egypt and Carboniferous of England." Geologia Croatica **56**(1): 19-37.

Tucker, M. E., et al. (2009). "Are beds in shelf carbonates millennial-scale cycles? An example from the mid-Carboniferous of northern England…." Sedimentary Geology **214**(1): 19-34.

Vail, P. R., et al. (1977). "Seismic Stratigraphy and Global Changes of Sea Level: Part 4. Global Cycles of Relative Changes of Sea Level.: Section 2. Application of Seismic Reflection Configuration to Stratigraphic Interpretation."

Ver Straeten, C. A., et al. (2011). "Mudrock sequence stratigraphy: a multi-proxy (sedimentological, paleobiological and geochemical) approach, Devonian Appalachian Basin." Palaeogeography, Palaeoclimatology, Palaeoecology **304**(1): 54-73.

Wanless, H. R. (1979). "Limestone response to stress: pressure solution and dolomitization." Journal of Sedimentary Research **49**(2).

Wei, G., et al. (2006). "Geochemical record of chemical weathering and monsoon climate change since the early Miocene in the South China Sea." Paleoceanography **21**(4).

Wei, G., et al. (2003). "Climatic impact on Al, K, Sc and Ti in marine sediments: evidence from ODP Site 1144, South China Sea." Geochemical Journal **37**(5): 593-602.

Woo, J. and S. K. Chough (2007). "Depositional processes and sequence stratigraphy of the Jigunsan Formation (Middle Ordovician), Taebaeksan Basin, mideast Korea: implications for basin geometry and sequence development." Geosciences Journal **11**(4): 331-355.

Wright, V. P. and T. P. Burchette (1998). "Carbonate ramps: an introduction." Geological Society, London, Special Publications **149**(1): 1-5.

Yin, A. and S. Nie (1993). "An indentation model for the North and South China collision and the development of the Tan-Lu and Honam fault systems, eastern Asia." Tectonics **12**(4): 801-813.

Zecchin, M. and O. Catuneanu (2013). "High-resolution sequence stratigraphy of clastic shelves I: units and bounding surfaces." Marine and Petroleum Geology **39**(1): 1-25.

Zhao, M.-Y. and Y.-F. Zheng (2014). "Marine carbonate records of terrigenous input into Paleotethyan seawater: geochemical constraints from Carboniferous limestones." Geochimica et Cosmochimica Acta **141**: 508-531.

Zhao, M.-Y. and Y.-F. Zheng (2015). "The intensity of chemical weathering: Geochemical constraints from marine detrital sediments of Triassic age in South China." Chemical geology **391**: 111-122.

Zhu, M.-Y., et al. (2004). "Evolution of C isotopes in the Cambrian of China: implications for Cambrian subdivision and trilobite mass extinctions." Geobios **37**(2): 287-301.

박태윤, et al. (2010). "동점 지역 대기층 상부의 각력에서 산출된 삼엽충 화석군의 의미." 고생물학회지 **26**(2): 173-181.

이병수 (2012). "강원도 영월의 마차리 단면 (마차리층) 에서 산출된 캄브리아기의 전기 푸롱통 (Furongian Series) 코노돈트 화석군." 고생물학회지 **28**(1-2): 11-27.

정직한 and 최덕근 (2007). "영월군 북면 갈골 마차리층에서 산출된 후기 캄브리아기 삼엽충 Pseudagnostus josepha (Hall, 1863) 의 개체발생과정과 형태학적 분석." 고생물학회지 **23**(1): 93-103.

최덕근 (2011). "태백산분지의 전기 고생대 고지리・고환경에 관한 새로운 견해." 고생물학회지 **27**(1): 1-11.

국문초록

태백산분지 내 태백지역의 세송, 화절층과 영월지역의 마차리층은 캄브리아 3기부터 푸롱지안에 걸쳐 혼합된 탄산염 쇄설성 환경에서 퇴적되었다. 이에 대해 순차층서학과 화학층서를 연구하였다. 퇴적상 분석을 통해 세송층과 화절층은 9개의 암상, 마차리층은 7개의 암상으로 분류하였다. 퇴적상 조합과 순차층서학적 경계면에 따라 세송층과 화절층은 3개의 시퀀스와 2개의 시퀀스 경계면으로 구성되어 있는 것으로 해석되었다. 마차리층은 2개의 시퀀스와 1개의 시퀀스 경계면으로 해석된다. 마차리층에서의 산화 환원 환경을 지시하는 미량원소 분석과 세송층과 화절층에서의 전체 암석의 탄소안정동위원소 분석은 상대 해수면 변화를 지시하며, 이는 순차층서학적 해석과 일치한다. 태백지역의 세송층, 화절층과 영월지역의 마차리층은 중국 산동 지방의 구샨층, 챠오미디안 층과 순차층서, 화학층서, 생층서적으로 잘 대비된다. 두 지역 간의 대비는 혼합된 탄산염 쇄설성 환경의 안정된 내륙해 내에서 대비가 가능함을 지시한다. 이 지역에 대한 순차층서학적 해석은 탄산염 생산성과 쇄설성 퇴적물의 유입 간의 상호작용이 기존의 탄산염, 쇄설성 퇴적 환경에 대한 모델 보다 더 복잡함을 제시한다.

주요어: 캄브리아기, 혼합된 탄산염 쇄설성 환경, 안정된 내륙해, 순차층서학,

화학층서, 안정탄소동위원소, 산화 환원 지시 미량원소, 쇄설성 퇴적물 유입, 탄산염 생산성